EEG SYSTEMS LABORATORY

1855 Folsom Street
San Francisco, CA 94103
415•621—8343

NEUROCOGNITIVE PREDICTORS OF PERFORMANCE

FINAL REPORT

AFOSR Contract F49620-84-K-0008
24 MAR 84 TO 23 AUG 87

PREPARED FOR

Dr. A. R. Fregly
Directorate of Life Sciences
Air Force Office of Scientific Research
Bolling AFB, D.C. 20332

APPROVED BY

Alan S. Gevins, Director

UNCLASSIFIED
SECURITY CLASSIFICATION OF THIS PAGE

AD-A188 323

REPORT DOCUMENTATION PAGE

Form Approved OMB No. 0704-0188

1a. REPORT SECURITY CLASSIFICATION: UNCLASSIFIED	1b. RESTRICTIVE MARKINGS
2a. SECURITY CLASSIFICATION AUTHORITY	3. DISTRIBUTION/AVAILABILITY OF REPORT: APPROVED FOR PUBLIC RELEASE, DISTRIBUTION UNLIMITED
2b. DECLASSIFICATION/DOWNGRADING SCHEDULE	
4. PERFORMING ORGANIZATION REPORT NUMBER(S): AFOSR03	5. MONITORING ORGANIZATION REPORT NUMBER(S): AFOSR-TR- 87-1593
6a. NAME OF PERFORMING ORGANIZATION: EEG SYSTEMS LABORATORY; 6b. OFFICE SYMBOL (If applicable):	7a. NAME OF MONITORING ORGANIZATION: DIRECTORATE OF LIFE SCIENCES, AFOSR
6c. ADDRESS (City, State, and ZIP Code): 1855 Folsom Street, Rm 610, San Francisco, CA 94103	7b. ADDRESS (City, State, and ZIP Code): Building 410, Bolling AFB, DC 20332
8a. NAME OF FUNDING/SPONSORING ORGANIZATION: AFOSR; 8b. OFFICE SYMBOL (If applicable): NL	9. PROCUREMENT INSTRUMENT IDENTIFICATION NUMBER: F49620-84-K-0008
8c. ADDRESS (City, State, and ZIP Code): Building 410, Bolling AFB, DC 20332	10. SOURCE OF FUNDING NUMBERS: PROGRAM ELEMENT NO. 61102F; PROJECT NO. 2313; TASK NO. A4; WORK UNIT ACCESSION NO. -

11. TITLE (Include Security Classification): NEUROCOGNITIVE PREDICTORS OF PERFORMANCE

12. PERSONAL AUTHOR(S): ALAN S. GEVINS

13a. TYPE OF REPORT	13b. TIME COVERED	14. DATE OF REPORT (Year, Month, Day)	15. PAGE COUNT
FINAL	FROM 24MAR84 TO 23AUG87	870925	65

16. SUPPLEMENTARY NOTATION

17. COSATI CODES			18. SUBJECT TERMS (Continue on reverse if necessary and identify by block number)
FIELD	GROUP	SUB-GROUP	SUBJECT TERMS LISTED ON PAGE 3
0508			
0509			

19. ABSTRACT (Continue on reverse if necessary and identify by block number)

Our aim is to measure the functional neural networks responsible for human goal-directed behaviors. During the past three years we developed new methods for recording and analyzing the electrical activity of the brain while subjects perform simple cognitive tasks. We have sought to determine the feasibility of predicting decrements in performance associated with transient attentional lapses or operational fatigue. Using the method of Event-Related Covariance (ERC) analysis, we found distributed neural "preparatory sets" that predicted the accuracy of subsequent responses. In a second experiment on the effects of operational fatigue in U.S. Air Force test pilots, we found fatigue-related neuroelectric changes during cognitive processing that preceded appreciable degradations in performance. These results suggest the feasibility of on-line systems that warn of impaired performance due to prolonged mental work by persons engaged in critical or hazardous work.

20. DISTRIBUTION/AVAILABILITY OF ABSTRACT	21. ABSTRACT SECURITY CLASSIFICATION	
☐ UNCLASSIFIED/UNLIMITED ☒ SAME AS RPT. ☐ DTIC USERS	UNCLASSIFIED	
22a. NAME OF RESPONSIBLE INDIVIDUAL: DR. A. R. FREGLY	22b. TELEPHONE (Include Area Code): (202) 767-5021	22c. OFFICE SYMBOL: AFOSR/NL

DD Form 1473, JUN 86 *Previous editions are obsolete.* SECURITY CLASSIFICATION OF THIS PAGE

UNCLASSIFIED

AFOSR-TR- 87-1593

SUPPLEMENT TO FORM DD1473 SECURITY CLASSIFICATION: UNCLASSIFIED

SECTION 18: SUBJECT TERMS

brain models
cognition
current source density
digital signal processing
EEG
event-related covariance
evoked potentials
functional neuroanatomy
human performance
Laplacian Derivation
magnetic resonance imaging
magnetoencephalgoram
neural-networks
operational fatigue
P300
parallel processing
pattern recognition
performance prediction
preparatory sets
spatial deconvolution
spatiotemporal analysis
Wigner distribution
working memory

Approved for public release;
distribution unlimited.

TABLE OF CONTENTS

Page

LIST OF FIGURES

Page

Page

I. OVERVIEW

A. Senior Scientific Personnel of the EEG Systems Laboratory
(* Indicates no longer with laboratory due to funding cutbacks.)

Steven L. Bressler, Neurophysiologist
* Brian A. Cutillo, Cognitive Scientist
* Joseph C. Doyle, Biophysicist
Alan S. Gevins, Director
Douglas S. Greer, Computer Scientist
Judy Illes, Neuropsychologist
Nelson H. Morgan, Electrical Engineer
Ronald K. Stone, Neurologist and Psychiatrist
Roseann Fowler-White, Operations Manager
* Gerald M. Zeitlin, Computer Systems Engineer

B. Publications

1. Gevins, A.S. & Morgan, N.H. (1984) Ignorance-based systems. *Proc. IEEE Int. Conf. Acoustics, Speech & Signal Processing, 3*, pp. 39A5.1-39A5.4.

2. Gevins, A.S. (1984) Analysis of the electromagnetic signals of the human brain: Milestones, obstacles and goals. *IEEE Trans. Biomed. Enginr., BME-31(12)*, pp. 833-850.

3. Gevins, A.S., Doyle, J.C., Cutillo, B.A., Schaffer, R.E., Tannehill, R.S. & Bressler, S.L (1985) Neurocognitive pattern analysis of a visuospatial task: Rapidly-shifting foci of evoked correlations between electrodes. *Psychophysiol., 22(1)*, pp. 32-43.

4. Gevins, A.S. (1986) Quantitative human neurophysiology. In: H.J. Hannay, (Ed.), *Experimental Techniques in Human Neuropsychology*. New York, Oxford University Press, pp. 419-456.

5. Gevins, A.S. (1986) Quantitative aspects of EEG and evoked potentials. In: M.J. Aminoff (Ed.), *Electrodiagnosis in Clinical Neurology*. New York, Churchill-Livingstone, pp. 149-203.

6. Gevins, A.S. & Cutillo, B.C. (1986) Signals of cognition. In: F. Lopes da Silva, W. Storm van Leeuwen & A. Remond (Eds.), *Handbook of Electroencephalography and Clinical Neurophysiology, Vol. 2: Clinical Applications of Computer Analysis of EEG and other Neurophysiological Signals*. Amsterdam, Elsevier, pp. 335-381.

7. Gevins, A.S., Morgan, N.H., Bressler, S.L., Doyle, J.C. & Cutillo, B.A. (1986) Improved event-related potential estimation using statistical pattern recognition. *Electroencephalogr. clin. Neurophysiol., 64*, pp. 177-186

8. Gevins, A.S. & Morgan, N.H. (1986) Classifier-directed signal processing in brain research. *IEEE Trans. Biomed. Enginr., BME-33,* pp. 1058-1064.

9. Morgan, N.H. & Gevins, A.S. (1986) Wigner distributions of human event-related brain potentials. *IEEE Trans. Biomed. Enginr., BME-33(1),* pp. 66-70.

10. Morgan, N.H. & Gevins, A.S. (1986) Ignorance-based signal estimation given multiple noisy realizations. *Proc. Int. Conf. on Acoustics, Speech, and Signal Processing (ICASSP-86),* Tokyo.

11. Gevins, A.S., Morgan, N.H., Bressler, S.L., Cutillo, B.A., White, R.M., Illes, J., Greer, D.S., Doyle, J.C. & Zeitlin, G.M. (1987) Human neuroelectric patterns predict performance accuracy. *Science, 235,* pp. 580-585.

12. Gevins, A.S. (1987) Overview of computer analysis. In: A.S. Gevins & R. Remond (Eds.), *Handbook of Electroencephalography and Clinical Neurophysiology, Vol.1: Methods of Analysis of Brain Electrical and Magnetic Signals.* Amsterdam, Elsevier, pp. 31-83.

13. Gevins, A.S. (1987) Correlation Analysis. In: A.S. Gevins & A. Remond (Eds.), *Handbook of Electroencephalography and Clinical Neurophysiology, Vol.1: Methods of Analysis of Brain Electrical and Magnetic Signals.* Amsterdam, Elsevier, pp. 171-193.

14. Gevins, A.S. (1987) Statistical pattern recognition. In: A.S. Gevins & R. Remond (Eds.), *Handbook of Electroencephalography and Clinical Neurophysiology, Vol.1: Methods of Analysis of Brain Electrical and Magnetic Signals.* Amsterdam, Elsevier, pp. 541-582.

15. Gevins, A.S. (1987) Obstacles to progress. In: A.S. Gevins & A. Remond (Eds.), *Handbook of Electroencephalography and Clinical Neurophysiology, Vol.1: Methods of Analysis of Brain Electrical and Magnetic Signals.* Amsterdam, Elsevier. pp. 665-673.

16. Gevins, A.S. & Morgan, N.H. (1987) "Ignorance- based" neural-network signal processing in brain research. *Proc. 1st Internat. Conf. Neural Networks,* San Diego.

17. Gevins, A.S. (1987) How the human brain thinks and acts: Results of latest research using neural net-works to analyze brain signals. *Proc. First Intern. Conf. Neural Networks,* San Diego.

18. Gevins, A.S. (In Press) Recent advances in neurocognitive pattern analysis. In: E. Basar (Ed.), *Dynamics of Sensory and Cognitive Processing of the Brain.* New York, Oxford University Press.

19. Gevins, A.S. (In Press) Analysis of multiple lead data. In: J. Rohrbaugh, R. Johnson, R. Parasuraman (Eds.), *Event-Related Potentials of the Brain.* New York, Oxford University Press.

20. Gevins, A.S., Cutillo, B.A., Bressler, S.L., Morgan, N.H., Fowler-White, R.M., Greer, D.S., Illes, J., Doyle, J.C., Tannehill, R.S., Zeitlin, G.M. (In Press) Neurophysiological precursors of accurate visuomotor performance. *Proc. NATO Aerospace Medical Panel Symposium,* Trondheim, Norway.

21. Gevins, A.S., Cutillo, B.A., Fowler-White, R.M., Illes, J. & Bressler, S.L. (In Press) Neurophysiological patterns of operational fatigue: Preliminary results. *Proc. NATO Aerospace Medical Panel Symposium,* Trondheim, Norway.

22. Gevins, A.S., Morgan, N.H., Bressler, S.L., Greer, D.S., Costales, B., Smith, K. & Faucette, R. (In Press) Fourth generation neurocognitive pattern analysis system. *Proc. NATO Aerospace Medical Panel Symposium,* Trondheim, Norway.

23. Gevins, A.S., Cutillo, B.A., Morgan, N.H., Bressler, S.L., Illes, J., White, R.M. & Greer, D.S. (In Press) Event-related covariances of a bimanual visuomotor task. In: R. Johnson (Ed.), *Current Research in Event-Related Brain Potentials.* Amsterdam, Elsevier.

24. Gevins, S.A., Bressler, S.L., Morgan, N.H., Cutillo, B.A., White, R.M., Greer, D. & Illes, J. (Submitted) Event-related covariances during a bimanual visuomotor task, Part I: Methods and analysis of stimulus- and response-locked data. *Electroencephalogr. clin. Neurophysiol.*

25. Gevins, A.S., Cutillo, B.A., Bressler, S.L., Morgan, N.H., White, R.M., Illes, J. & Greer, D. (Submitted) Event-related covariances during a bimanual visuomotor task, Part II: Preparation and feedback. *Electroencephalogr. clin. Neurophysiol.*

26. Gevins, A.S., Stone, R.K., Ragsdale, S.D. (Submitted) Differentiation of the effects of three benzodiazapines on non-REM sleep EEG spectra using neural-network pattern classification analysis. *Psychopharmacology.*

II. OBJECTIVES & SIGNIFICANCE

A. General

We continue to develop new methods for recording and analyzing the electrical activity from the brain of people performing simple cognitive tasks. Our goal is to accurately measure the distributed functional neural networks responsible for human goal-directed behaviors.

Our short-term objective is to predict decrements in performance consequent to attentional lapses or operational fatigue. Our long-term objective is to develop an instrument to non-invasively measure the functional neuroanatomy of the human brain with high temporal resolution. Such an instrument would be invaluable for neuropsychological studies of cognition, including assessment and training of cognitive skills, for clinical studies such as monitoring recovery of function following head injury, and for on-line monitoring of attention such as detecting transient cognitive impairments or G-induced loss of consciousness in the cockpit.

B. Specific

Recordings with up to 64 scalp EEG channels during highly controlled tasks are now routine in our laboratory, as is the sequence of signal processing operations required to extract neurocognitive information from sets of single-trial data comprising up to several billion bytes. More robust measures of the "functional interdependency" between electrodes (event-related covariance — ERC) have been developed and applied to data from a bimanual visuomotor task recorded several years ago. The results of that experiment were clear-cut and consistent with neuropsychological models of the cortical activity accompanying expectancy, stimulus registration and feature extraction, movement preparation and execution, and feedback (see Section IV.A). Many of these results, along with pilot analyses of intracerebral recordings using a primate model, cannot be explained by single equivalent-current dipole source models, but could be understood in the context of multiple, simultaneously active neuronal sources. Determining multiple neuronal sources associated with cognitive processing remains a formidable problem, however, since the projected patterns of scalp potential from those sources overlap both in time and in space, and are usually smaller than unrelated spontaneously-generated brain potentials.

Since the main, unresolved issue is the origin of ERC patterns measured at the scalp, we are now concentrating on improving our ability to relate scalp recordings to source generator configurations. With improved technologies currently available, we believe that several simultaneous sources can be resolved.

III. METHODOLOGICAL ADVANCES

A. Overview of Neurocognitive Pattern (NCP) Analysis

Thus far, there have been four generations of NCP Analysis. The first measured background EEG spectral intensities while people performed complex tasks, such as arithmetic problems lasting up to one minute. Complex perceptuo-motor and cognitive activities like these produce unique, spatially differentiated scalp EEG spectral patterns. These patterns had sufficient specificity to identify the type of tasks being performed [1-3]. These results agreed with previous reports of hemispheric lateralization of "spatial" and "linguistic" processing. But when the tasks were controlled for stimulus, response and performance-related factors, they had identical, spatially diffuse EEG spectral scalp distributions [4] (Fig. 1). Since no patterns of hemispheric lateralization were found, this suggested that previous and most current reports of EEG hemispheric lateralization may have confounded electrical activity related to limb and eye movements and arousal with those of mental activity.

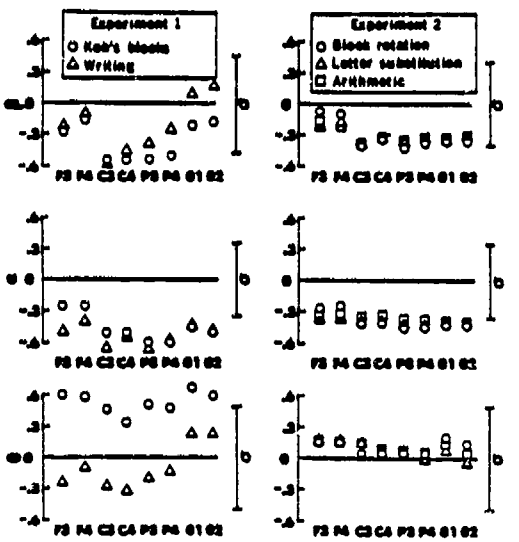

Figure 1

Results of experiments designed to assess EEG correlates of complex cognitive functions. The graphs display means over all subjects of standard scores of EEG spectral intensities (expressed as changes from visual fixation values for clarity of display) recorded during performance of two tasks in Experiment 1 and three tasks in Experiment 2. Upper, middle and lower sets of graphs are for spectral intensities in the theta, alpha, and beta bands. The abscissae show scalp electrode placements: F3, left frontal; F4, right frontal; C3, left central; C4, right central; P3, left parietal; P4, right parietal; O1, left occipital; and O2, right occipital. Standard deviations, which differed only slightly between electrode placements, are indicated at the right of each graph. (Left) Tasks of Experiment 1 were one minute long and involved limb movements and uncontrolled differences in stimulus characteristics and performance-related factors. (Right) Tasks of Experiment 2 were less than 15 seconds long and required no motion of the limbs; stimulus characteristics and performance-related factors were also relatively controlled. Although there are prominent EEG differences between the uncontrolled tasks of Experiment 1, EEG differences between the relatively controlled tasks of Experiment 2 are lacking. Each of the controlled tasks is, however, associated with a remarkably similar bilateral reduction in alpha and beta spectral intensity over occipital, parietal, and central regions [3].

The second generation of NCP Analysis measured crosscorrelations between 91 pairwise combinations of 15 electrodes recorded during performance of simple tasks. These split-second tasks, controlled so that only the type of judgment varied, were associated with complex, rapidly-shifting event-related correlation patterns [5] (Fig. 2). By extracting differences between similar spatial tasks, rapidly shifting focal patterns were found that were in agreement with the known functional neuroanatomy of the cerebral cortex [6,7] (Fig. 3). From these results, it was clear that it was possible to measure salient aspects of the rapidly shifting, complex mass neural processes that are associated with the successive information processing stages of simple visuomotor judgment tasks.

The third generation involved expansion of the recording and analysis systems to operate on up to 64 channels. The task protocol was developed to allow a controlled sequence of stimuli in which a person prepared for, and executed, perceptual judgment and motor response tasks, and received performance feedback.

The fourth and latest version of NCP Analysis (ADIEEG-IV) includes many significant operational improvements (Fig. 4) [8]. It has a greatly expanded capacity and its operation is being automated by development of an AI expert system. It is designed for up to 256 channels, and is implemented on a 32-bit multiprocessor system which currently has 3 computing nodes, a 6 million floating-point-operations-per-second capability and a 3500 megabyte on-line disk capacity.

The data acquisition system is capable of sampling up to 256 channels at up to 2 kHz sampling rates per channel. (Current amplification capabilities are 128 channels.) Trial presentation is automatically delayed until eye blinks, amplifier settling from eye blinks, and gross body movements have all ended. Up to 70 EEG and non-EEG channels are monitored at a time on a color graphics screen to detect electrode problems. Other channels are bank-switchable to the monitor. Averages can also be viewed on-line to check for event-registered artifacts.

Off-line, an interactive graphics trial editing program is used by an operator to check the decisions of the automatic on-line artifact detectors. In practice, editors have become sufficiently skilled to check the single trials of an experiment in roughly the time that it takes to run the experiment. (This represents a speed-up of 10-15 times over previous manual procedures.)

A Laplacian spatial filter can be applied using precise measurements of electrode position to remove the effect of choice of reference channel and reduce spatial blur [10]. Additionally, a pathway has been built for the inclusion of detailed structural information via reconstruction of actual scalp, skull, and brain geometries using Magnetic Resonance (MR) images (Fig. 5). This information is used to deblur average event-related potential waveforms to estimated currents leaving the brain (actually, a smooth hypothetical surface surrounding the brain).

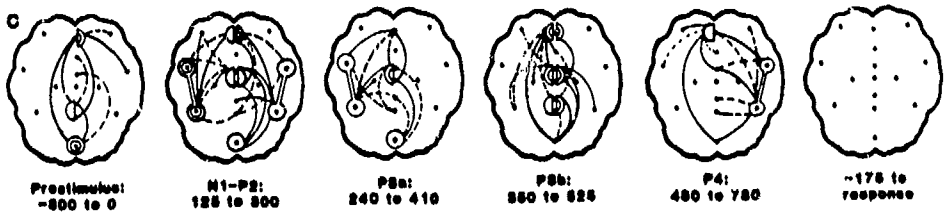

Figure 2

Spatiotemporal brain potential differences between two split-second tasks, one requiring a spatial judgment and the other requiring a numeric judgment, are shown in each of six intervals from just before the stimulus to just before the response. A pressure of the right index finger was the required response in both cases. The most significantly differing electrodes are shown by circles (connected when grouped in pairs), their significance level by stippling of the circles, and their most prominent correlations with other electrodes by inter-electrode lines. A solid line between two electrodes indicates that the correlation between the electrodes was higher in the spatial task, while a dotted line indicates higher numeric task correlations.

Note the contrasts between the spatial and numeric tasks in the prestimulus interval, a finding that might be interpreted as evidence of a "preparatory set." Also, the lack of contrast in the preresponse interval may be interpreted as the completion of task-specific perceptual processing [6].

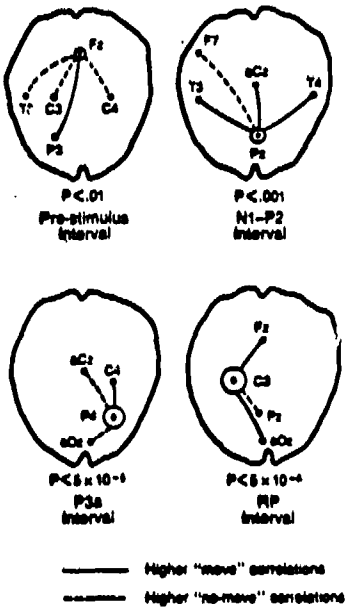

Figure 3

Spatiotemporal brain potential differences occurring between two split-second spatial tasks in each of four intervals from just before the stimulus to just before the response. The "Move" task required a pressure of the right index finger, while the "No-Move" task required withholding the response. The size of the circle in each interval is proportional to the significance of between-task differences at the most significant electrode in that interval (i.e., Fz<.01, Pz<.001, P4<.00005, C3<.000005). A solid line between two electrodes indicates that the correlation was higher in the "Move" task, while a dotted line indicates higher "No-Move" task correlations. The midline frontal (Fz) electrode focus in the prestimulus interval suggests a differential preparatory set; the midline parietal (Pz) focus in the interval centered on the N1 and P2 evoked potential peaks suggests task-specific feature extraction and pattern recognition; the right parietal (P4) focus in the interval centered on the P3a evoked potential peak suggests differential spatial judgments between the "Move" and the "No-Move" tasks, while the left-centered (C3) focus in the pre-response interval suggests preparation of the right index finger response in the "Move" task [6,7].

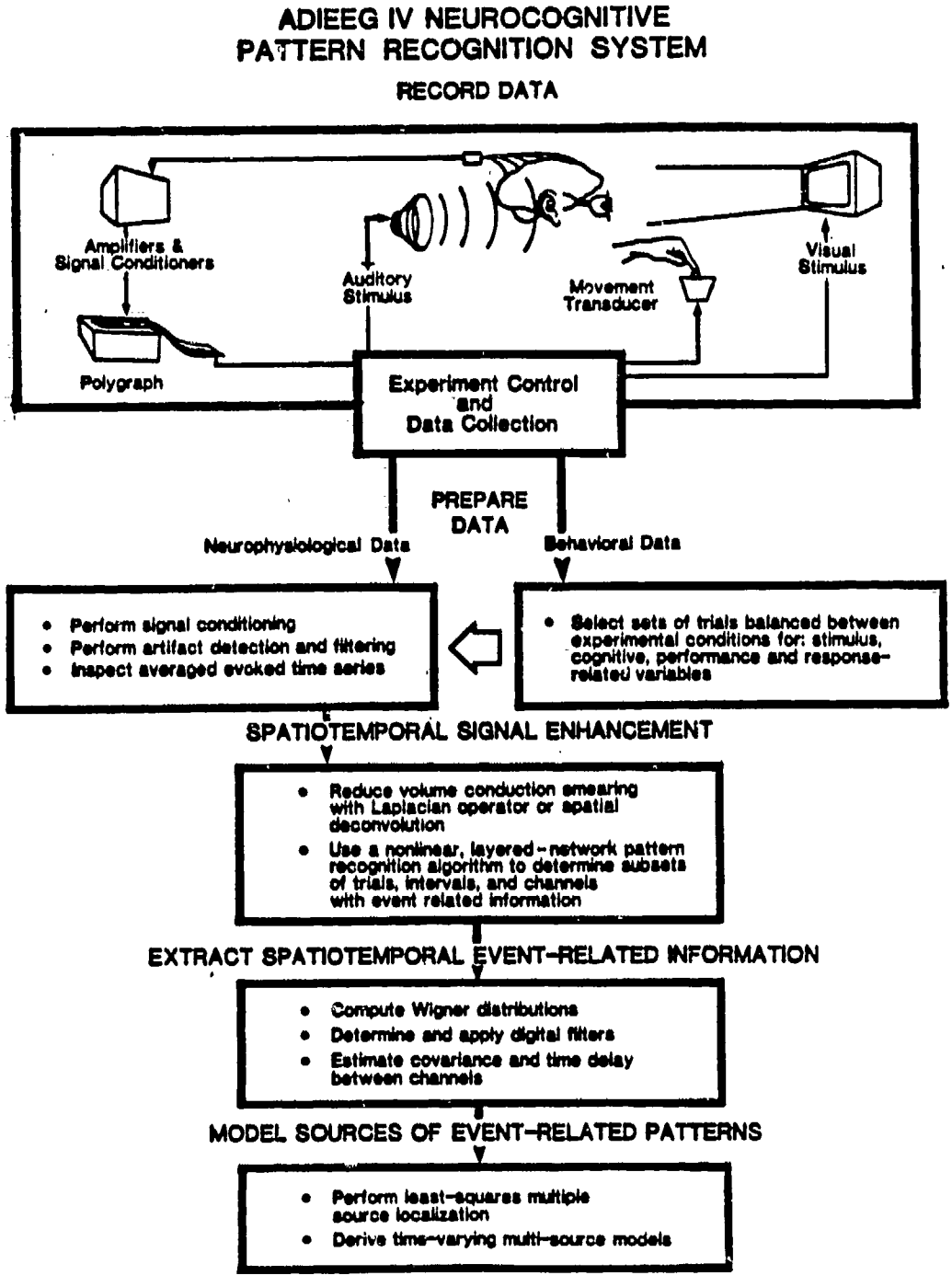

Figure 4

The ADIEEG-IV system for quantification of event-related brain signals is shown. Separate subsystems perform on-line experimental control and data collection, data selection and evaluation, signal processing and pattern recognition. Current capacity is 128 channels. Spherical-head spatial deblurring modules have been implemented, and multiple source modeling algorithms are being developed. Digital tapes of magnetic resonance images or of electrophysiological data from other laboratories are converted into the ADIEEG data format using gateway programs. The data are then processed using the same program modules as data collected in the EEG Systems Laboratory [9].

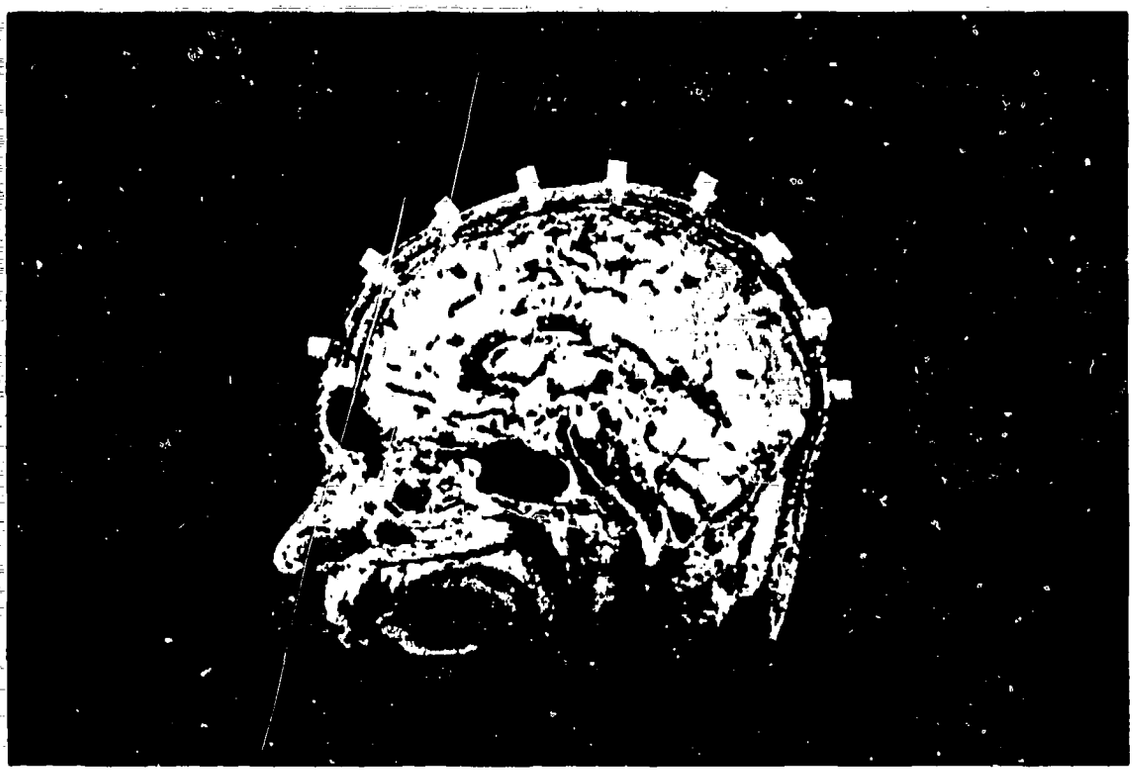

Figure 5

Magnetic Resonance Image of mid-sagittal section of a subject's cranium. EEG electrodes are superimposed [12].

The resulting sets of purified and selected EEG (or MEG, for imported data) trials are then entered into one of a number of possible single-trial or average event-related potential analyses. Averaging, filtering, time-varying spectral analysis, modeling, ERC measures, and multivariate pattern recognition are all supported under this system. Finally, two- and three-dimensional perspective plots are available to view the results of these analyses.

This system is currently being improved to provide greater ease of operation. While recording, channels that are not currently on-screen will nonetheless be automatically monitored for serious problems such as flattening or saturation. Additionally, other artifacts such as eye movement and muscle contamination will be automatically marked by on-line pattern classification programs (Fig. 6) [11]. Also, algorithms are under development to recover trials with non-saturating artifacts. Eye blinks or eye movements, for example, will be removed using least squares noise cancellation given EOG reference electrodes near the eyes. The system will then automatically calculate the optimum (largest) subset of trials that behaviorally balance for a requested set of variables on each split of the data

required to test an experimental hypothesis (e.g., between low and high accuracy trials). This will be followed by a manual check of the split distributions, along with corrections in exceptional cases. This will be speeded up by a convenient, window-oriented user interface. Further development of the analysis system will allow each step to be requested by the user without reference to file names or directory locations.

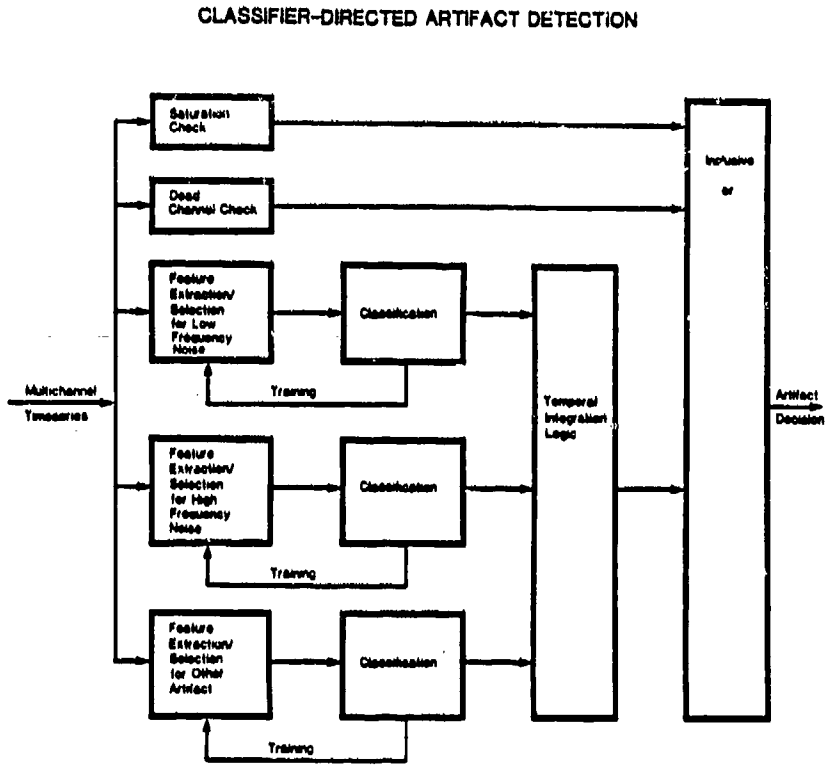

Figure 6

Classifier-directed artifact rejection. A system consisting of five parallel detectors is used to find contaminants. Three of the detectors incorporate layered-neural-network classifiers to choose and weight feature combinations. In this way, a precise automated procedure replaces sole reliance on *ad hoc* waveform detectors and subjectively determined thresholds [11].

B. Recent Developments in NCP Analysis

1. *Data Collection*

a. *64-channel EEG Recording Technique and Automated Artifact Rejection.* Recording capacity has been expanded to a full 64 EEG channel capacity to provide uniform scalp coverage with an interelectrode distance of about 3.25 cm on an adult head (Fig. 7). All recordings are referenced to one mastoid (usually M2); the other (M1) is recorded as a separate channel so that a laterally balanced (M1+M2) reference may be computed off-line, avoiding the undesirable boundary condition on the potential field created by linked-ear references. Signals are digitized at 12 bits full scale at 256 samples/sec, and stored on magnetic tape. Up to 70 channels are monitored at a time for electrode problems. Improved automated artifact rejection algorithms using neural-network pattern recognition to combine amplitude, frequency, and topographic features [11] are currently applied off-line, and are being converted to on-line analysis. These algorithms satisfactorily perform a preliminary data screening.

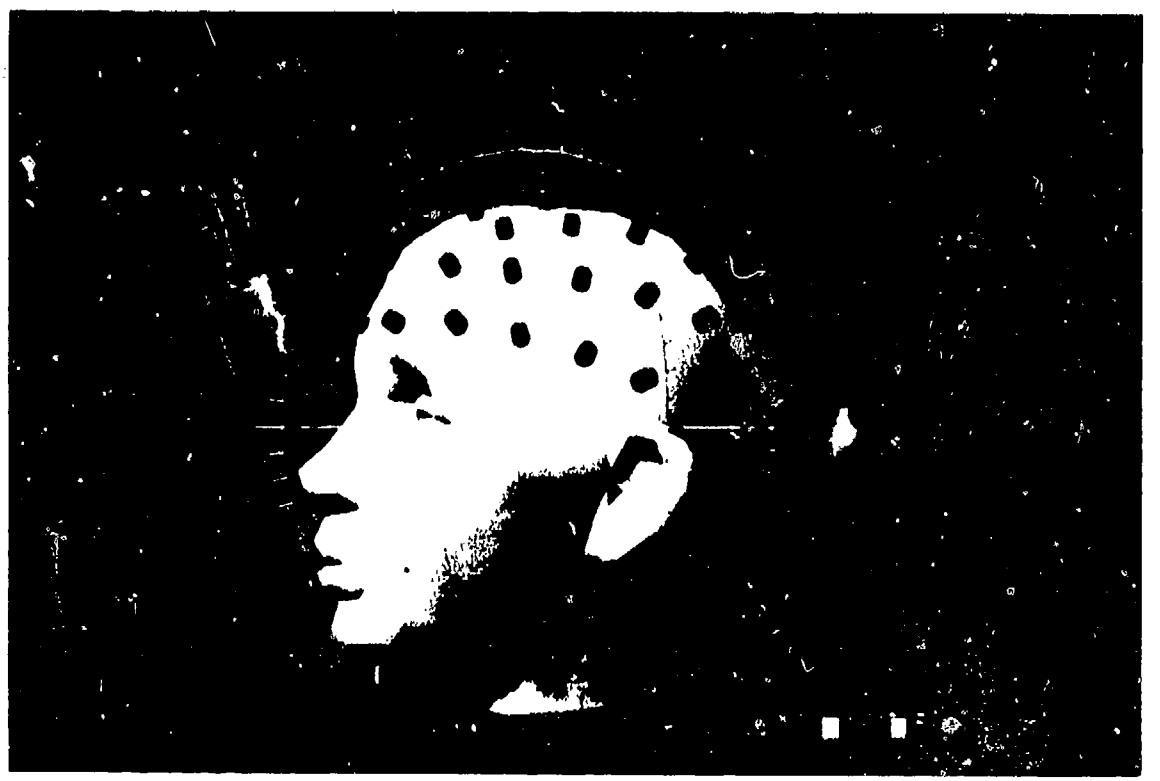

Figure 7

Expanded 10-20 System of electrode positions. Additional rows of electrodes, interpolated between the International 10-20 System coronal rows, have the letter a for "anterior" added to the designation for the next row anterior, e.g., aPz for anterior parietal midline electrode. With 64 electrodes, the average distance between electrodes on an adult head is ~3.25 cm [9].

Neural-network pattern classification techniques were used to evaluate the performance of two techniques for eye-movement-artifact removal: amplitude subtraction and spectral subtraction (Fig. 8). Although visual comparison showed that both methods are effective, the objective evaluation technique suggested that the spectral subtraction method may in some instances be more effective for eye blink removal.

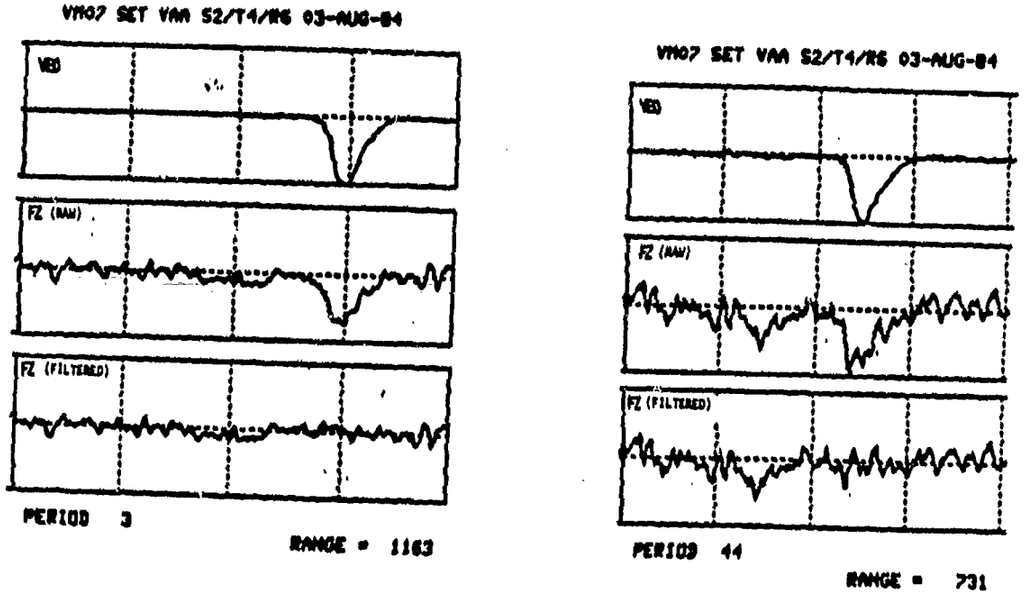

Figure 8

Two examples (left and right) of the application of a spectral eye-movement filter to large blink artifacts. The top row shows an eye blink recorded from the vertical eye movement channel, the middle shows the midline frontal EEG channel (F_Z) record contaminated by the blink, and the bottom shows the same EEG channel filtered to remove the eye blink contaminant [13].

b. *Digitization of Electrode Positions.* Before and after a recording session, the position of the external center of the grommet of each electrode is measured in three dimensions using a 3-D digitizer (Fig. 9). The participant rests his head in a padded stabilizing jig for the 5 minutes required to digitize the positions of all electrodes. Correction to scalp positions is made by a least-squares fit Multiple Linear Regression, which yields the general ellipsoid surface best fitted to the set of digitized positions, and the digitized coordinates are translated to a coordinate system centered on this ellipsoid.

c. *MR Imaging for Determining Positions of Electrodes and Cortical Structures.* Full sets of Magnetic Resonance Images (Fig. 10) are made at UCSF Long Hospital facility. These are high- resolution (0.8 mm pixel) 3-axis cross-section images of soft tissue 5 mm or 1 cm apart over the whole volume of the head. The pictures are digitized to give coordinate surfaces for scalp, outer and inner skull surfaces, and cerebral surface, including loci of major fissures. Comparison of electrode positions and MR measurements provides correlation of electrode positions and cortical areas, allowing comparison of functional neuroanatomy across individual participants for localized sensory and motor cortical ERP components. Direct measurement of scalp and skull thicknesses provides accurate information for use in spatial deconvolution (see below).

2. *Initial Data Analysis*

a. *Trial Selection Using Pattern Recognition.* A great deal of effort has been expended in attempts to form improved estimates of the averaged ERP (reviews in [14-17]). Most methods assume that task-related signals are present in every trial and also have inherent assumptions about the statistical properties of signal and noise. We have developed a method for ERP estimation without the first assumption and with a relaxed second assumption [18]. To do this, separate averages are formed from trials with and without detectable event-related signals. In the averages of trials with detectable signals, the ERP peaks are enhanced in comparison with the original averages. The averages of trials without detectable signals resemble the background EEG (Fig. 11).

Several dozen applications of this technique suggest that it is successful in identifying trials with a poor signal-to-noise ratio. The technique thus provides a simple method of ERP estimation with minimal *a priori* assumptions about the characteristics of the signal.

b. *Wigner (Time-Frequency) Distributions.* The ERP waveform is a function of time and does not provide explicit frequency information. Power spectra of ERP waveforms provide frequency information but obscure time-dependent phenomena. A view of the spectrum as it changes over time would give a new view of the evolution of different frequency components of the ERP. A simple approach would be to compute the spectrum over highly overlapped windows of the average ERP. However, such a "spectrogram" would smear together events within each analysis window. While there is an unavoidable trade-off between frequency and time resolution (known as the Heisenberg Uncertainty Principle), the spectrogram is an inflexible way of determining this choice.

Figure 9

EEGSL technician digitizing the positions of scalp electrodes. The total time for measuring all positions is approximately 5 minutes [13].

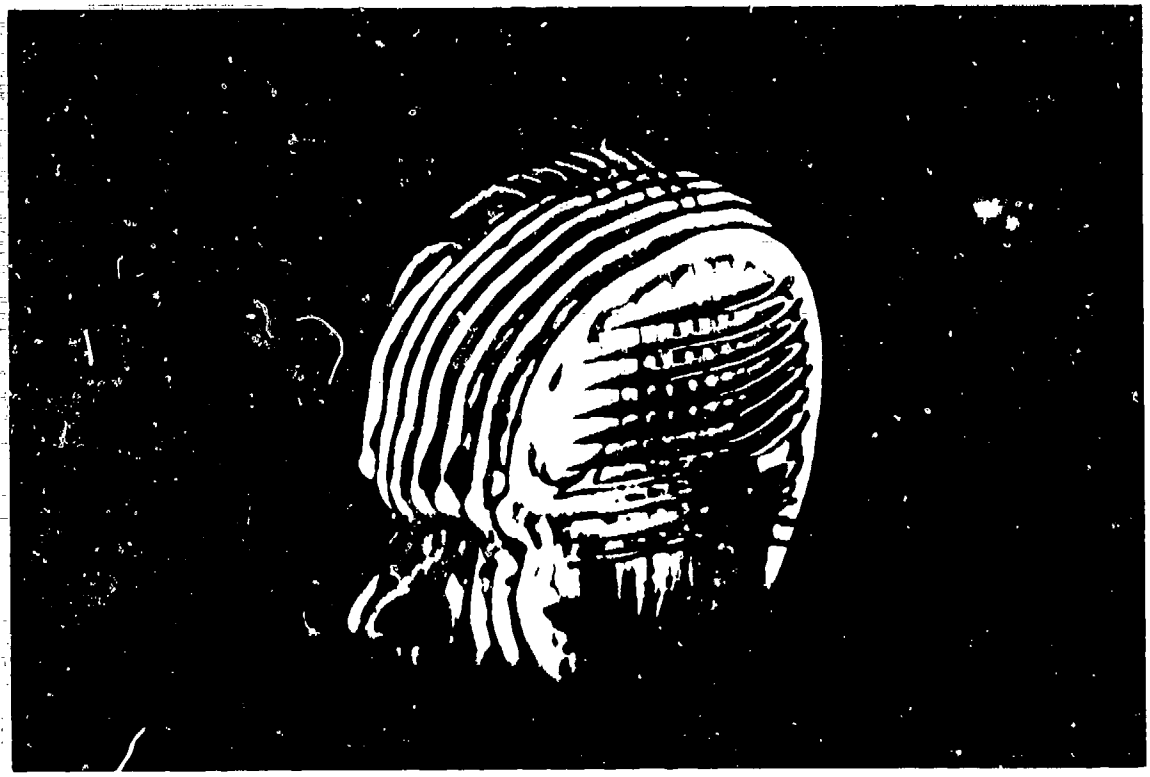

Figure 10

Composite of Magnetic Resonance Images of a participant's cranium recorded at 1 cm intervals in each of the three orthogonal directions.

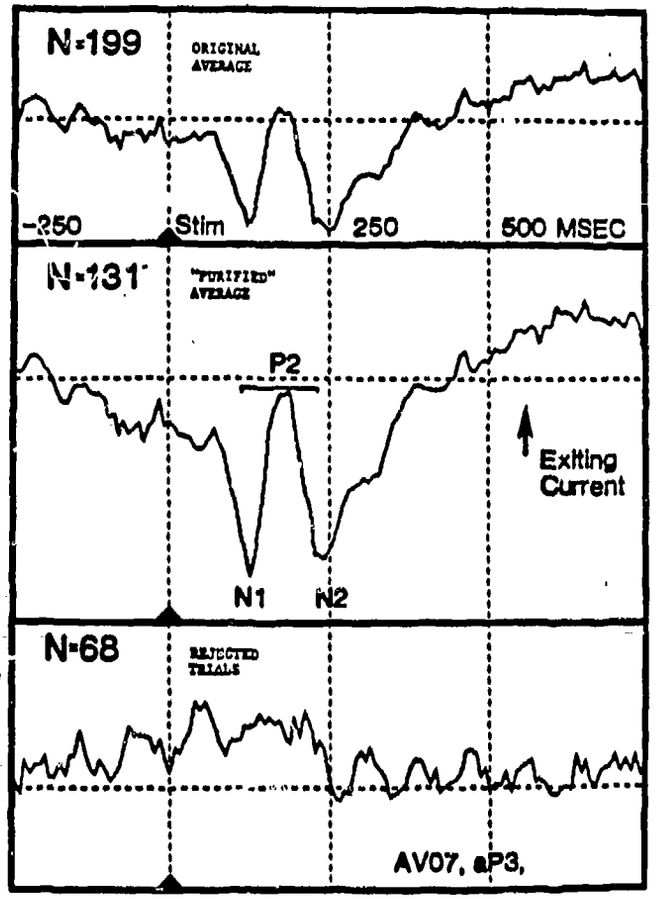

Figure 11

Use of statistical pattern recognition analysis to remove trials without detectable task-related signals from a set of single-trial ERPs (actually event-related current source densities). This results in an average ERP with a higher signal-to-noise ratio obtained from *fewer* trials. Unlike optimal filtering methods, *a priori* hypothesized models of the structure and statistical properties of signal and noise components are not required. (From [17,18].) (a) An original average ERP formed from 199 presentations of a visual numeric stimulus. (b) Average of 131 trials with consistent task-related signals in the P2 interval. Trials were selected from the original set of 199 by applying a pattern recognition algorithm to distinguish a 125-ms, P2 time series segment from a pre-cue "baseline" segment. Note the greatly increased size of the event-related peaks and lower frequency wave forms. (c) Average of 68 trials which did not have consistent task-related signals in the P2 interval. Note the relative lack of event-related activity and the dominance of ongoing EEG alpha waves.

A preferred method is to compute a general function of time and frequency called the Wigner Distribution [19-21] which approximates the instantaneous energy for a given time and frequency. In practice, ERPs often show strong enough energy "peaks" in the Wigner Distribution to validate very simple interpretations of the time and frequency locations of signal energy (Fig. 12). The Wigner Distributions are being used to determine digital filter characteristics which produce optimal time-frequency resolution for a given data set.

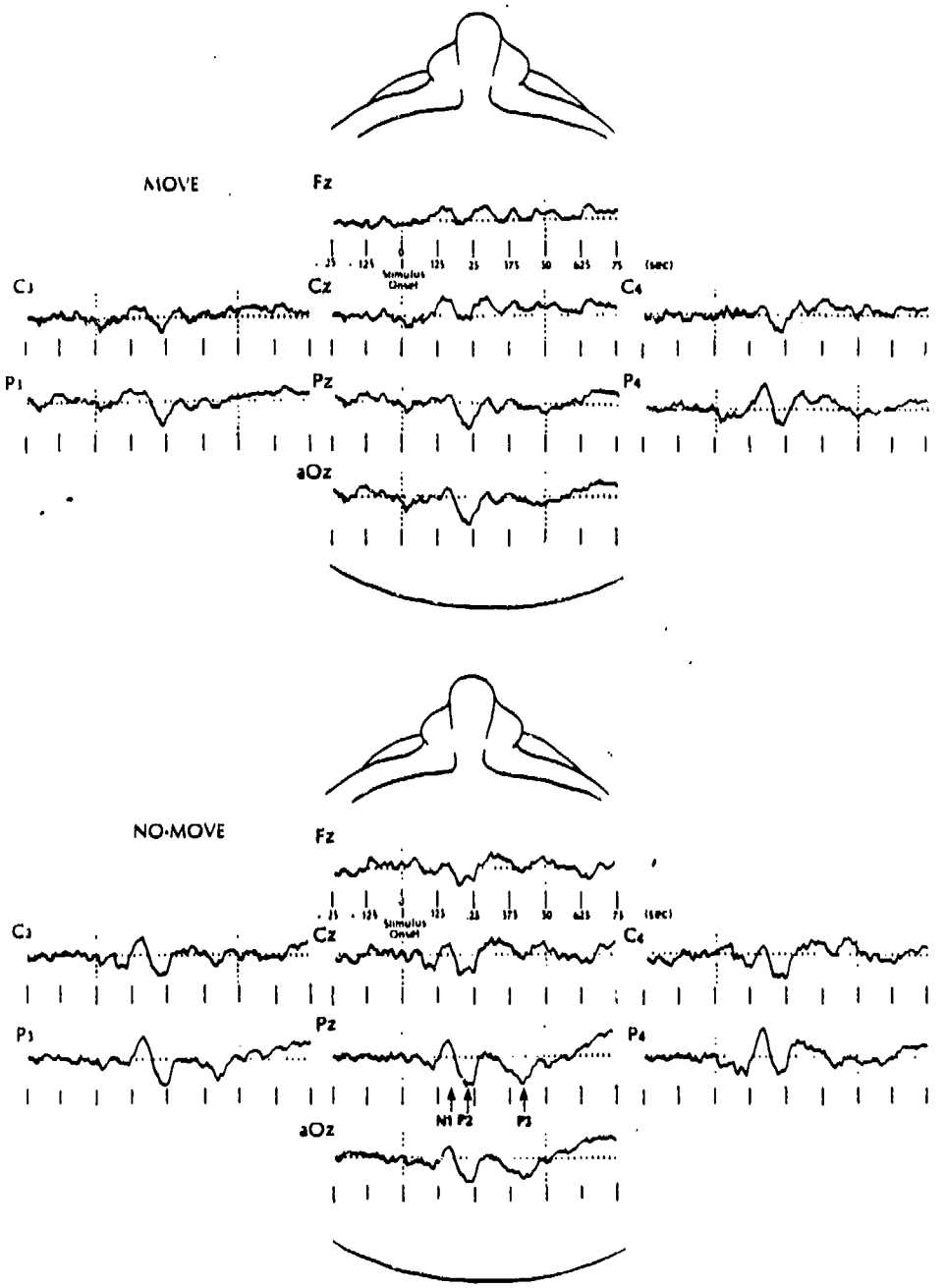

Figure 12a

Figure 12 gives two representations of eight average ERP channels for "move" and "no-move" cognitive tasks. The view is of the top of the head, with the nose at the top of each set of eight channels.

Figure 12a shows the average time series of 40 no-move and 37 move trials. These trials were selected by a statistical pattern recognition algorithm as having consistent task-related signals that differed between the move and no-move tasks. Three of the most commonly studied ERP peaks — N1, P2, P3 — are indicated on the Pz channel of the no-move task. Of these, the P3 peak is larger in the infrequently occurring no-move trials.

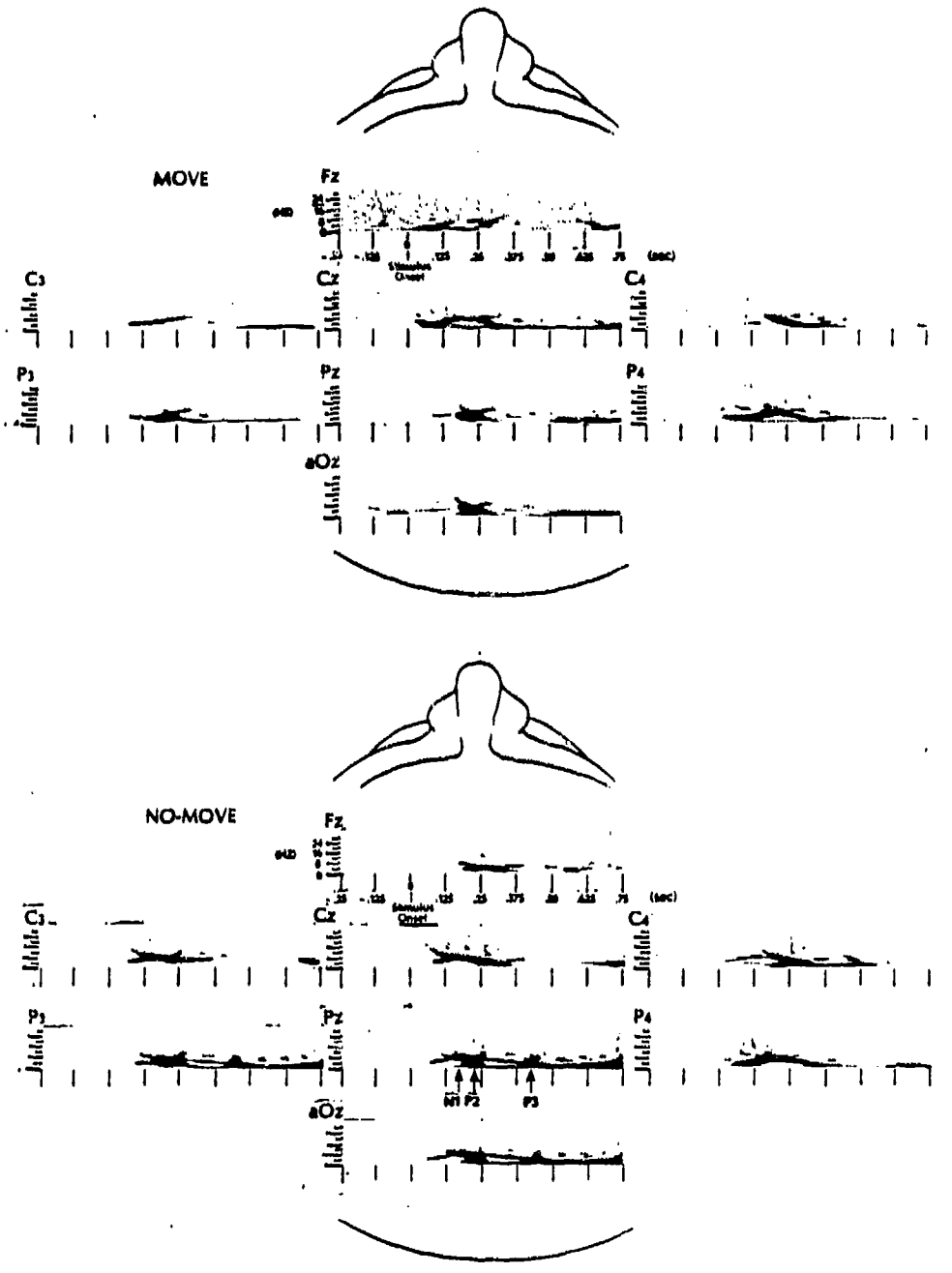

Figure 12b

The pseudo-Wigner distribution of the analytic signal of the same data. This representation shows that the event-related processes are changing rapidly in both time and frequency. The first moment along the time axis for each frequency is the group delay, while the first moment along the frequency axis is the instantaneous frequency. There is a buildup in energy after the stimulus, and a general increase in frequency until the energy concentration between the time of the N1 and P2 peaks begins to fall off (most prominent in the Pz channel). Then there is a glide down in frequency in the no-move task (most prominent in the Pz and aOz channels), which culminates in a concentration of energy around the time of the P3 peak. (From [19].)

c. *Balancing Data Sets.* Special attention is given to the preparation of data sets, since we believe that this is a highly neglected aspect of experimental control. In order to form balanced pairs of data sets for each neurophysiological hypothesis, the total set of artifact-free trials from each recording is submitted to an interactive program that displays the means, t-tests and histogram distributions of about 50 behavioral and other variables [7]. Pairs of data sets can be quickly inspected for significant differences in variables not related to the hypothesis and pruned of outlier trials until balanced, usually to a conservative alpha of .2. The program greatly facilitates the handling of large amounts of data and permits a high degree of control of stimulus, behavioral and other variables which would not otherwise be possible. It outputs labeled lists of trials to be submitted to the signal processing and analysis programs of our system that vary only according to the chosen hypothesis. Variables include stimulus parameters, responding finger, response onset and inter-movement times, response movement force, velocity, acceleration and duration, error and adaptive performance measure. There are also indices of eye movement and EMG activity computed in separate 500-msec epochs before and after the onset of cue, stimulus, response and feedback.

d. *EEG Spatial Signal Enhancement.* Attempts to study the information processing activity of the brain using scalp-recorded ERPs have suffered from the fact that potentials induced at the scalp by volume conduction from cerebral sources are subject to considerable distortion by the intervening media of cerebrum, cerebro-spinal fluid, skull, and scalp. The result is a smearing or spatial low-pass filtering of the pattern of activity in the brain. This section reviews two spatial filters that may increase the resolution of the recorded topographical map of brain activity: Laplacian Derivation and Deconvolution. Each provides a measure of the local density of normal current at the brain-skull surface due to the activity of neuronal sources within the brain. Each is independent of the reference electrode and applicable to single trials as well as to averages. Time series analysis and hypothesis testing may be performed on the filtered densities in identical fashion to potential maps.

The Laplacian Derivation (LD) [22-25], an estimate of the two-dimensional (tangential) Laplacian operator at each scalp position, is proportional to the local density of current flow through the skull. Its application has a localizing effect since it is a differential property of the potential field.

The other filter models the passive tissues of skull and scalp in order to deconvolve the measured scalp potential distribution into a topographical map of outgoing current density just above the surface of the cortex. This sheet of "dipoles" is equivalent to a "Helmholtz double layer" that completely characterizes the activities of the real sources within [26]. The surface of the cortex is chosen because all the neuronal sources are inside it. It must be stressed, however, that the deconvolved dipole density is not a model of sources in the sense that it will not "correct" the false impression of two radial sources created by a single tangential source. This deconvolution is similar in concept to a "software lens" applied by Freeman [27] to recordings from the surface of the olfactory bulb in the rabbit, although the same planar homogeneous model is not applicable to scalp-recorded data. It embodies the same principle as a treatment by Nicholas and DeLoche [28] of scalp-recorded ERPs. Since source modeling [29-31] requires an identical model

of the tissues outside the brain, this computationally cheap deconvolved current density may serve as a starting point for source modeling, with the effects of the passive tissue already removed.

Here we compare common average reference, Laplacian Derivation, and deconvolution procedures. The interchannel covariances for the three derivations are calculated on a visual ERP, as well as by a linear regression of interchannel covariance against the expected volume conduction. Additionally, simulation studies investigate the relative advantages of the filters as a function of electrode spacing.

Potentials were recorded from a right-handed adult male performing a task involving a brief, foveally presented, visual, single-digit numeric stimulus followed by a precise motor response (see Section IV.A). Fifty scalp electrodes were placed in an extension of the standard International 10-20 System, with additional coronal rows interpolated between the standard rows (see Section IV.A.1.c). Recording was done in bipolar chains of eight electrodes; digitized values were converted offline to a common average reference [32]. Electrode positions were measured using a stereophotogrammetry system developed for craniofacial research and treatment [33,34]. The Laplacian Derivation and deconvolution were implemented using the measured electrode coordinates to calculate the interelectrode distances. All data were edited for artifacts on a channel-by-channel basis by two independent experts.

The Laplacian Derivation estimate at each electrode was implemented as the average directional derivative divided by the average inverse distance. The latter quantity, however, may differ considerably in a practical montage. Worse, using this expression for electrodes on the periphery of the montage amounts to assuming that the average directional derivative on the outside is the same as that on the inside, which is hardly warranted in the absence of information.

A simple three-sphere head model was used for the deconvolution. The electric potential at each scalp position was the linear superposition (convolution) of contributions from all sources. If z is a vector expressing the scalp potential distribution, and x is a vector of "dipole" strengths, with H a matrix representing the transmission between cortical "dipoles" and scalp potentials, then this convolution may be written as

$$z = H\,x$$

The elements of the matrix H are calculated in the context of a particular model of the tissues by solving the boundary value problem governing the volume conduction between brain and scalp. The deconvolution was done using a standard model of the head as three concentric spheres: brain, skull, and scalp [24,28-31]. Discrete current dipoles representing an approximation to a continuous distribution of normal current are posited at the brain-skull boundary beneath each electrode. The values for the thicknesses of skull and scalp and the resistivities of the tissues were taken from standard sources [35-37].

Isofunction contour plots for common average, Laplacian Derivation (LD), and deconvolution are shown in Figure 13 for a single time point at an early peak of the averaged evoked potential. There is apparently more spatial detail in the Laplacian Derivation and deconvolution than in the common average. A similar result was apparent at the many different time points that were examined.

In practice there is noise n present in the measured scalp potentials z', $z' = z + n$. The matrix H may be singular or ill-conditioned, so that the inversion may require calculation of a pseudo-inverse or its equivalent using an orthogonal transformation. Use of scalp data from multiple time points in the vicinity of a peak in the evoked response may lead to a better estimate of x. Still, simple inversion of the convolution presented here is well conditioned, with the determinant of H equal to 15.4, and the condition number of the inversion equal to 34.4, corresponding to about 5 bits of noise. Householder inversion of 4 to 7 points in the vicinity of a peak produced topographical maps virtually identical to the simple inversion. A simple inversion is, therefore, considered adequate to the problem, given the other limitations of the model.

Like the Laplacian Derivation, the deconvolution has problems at the periphery of the recording electrode array. The model assumes that current outflow (or inflow) past the outer dipole positions makes a negligible contribution to the potential at each scalp electrode. In this implementation, values of Laplacian Derivation and deconvolved dipole density were treated with caution at the periphery.

For each derivation (common average, Laplacian Derivation, and deconvolution) covariances were calculated between all pairs of non-peripheral estimates on stimulus-locked averages from 0.5 sec before the stimulus to 1.0 second after. Such a covariance should primarily reflect the effects of volume conduction, since it spans intervals with different functional topography. Thus the point-spread function should be a good predictor of covariance for the common average derivation and a poor predictor for the others. A linear regression was performed to test this hypothesis.

Simulation calculations were performed to determine the response of each derivation to a single dipole source at a succession of positions. Using the three-sphere model described above, a single dipole was assumed at positions beginning at the cortex below Cz and progressing forward along the midline at 64 equal intervals of polar angle for a total of 0.8 radians. For each dipole position, the potential at each of the 50 measured electrode positions was calculated. For each such scalp potential distribution, the Laplacian Derivation and deconvolved source strength at Cz were calculated, as well as the potential at Cz.

In order to investigate the effect of closer electrode or dipole spacings, sets of position coordinates were prepared from the original measured set with all polar angles reduced to 0.75 and 0.5 of the originals. Thus all the interelectrode spacings were reduced proportionately. The responses of the Laplacian Derivation and deconvolution were calculated using these sets of coordinates for both source and

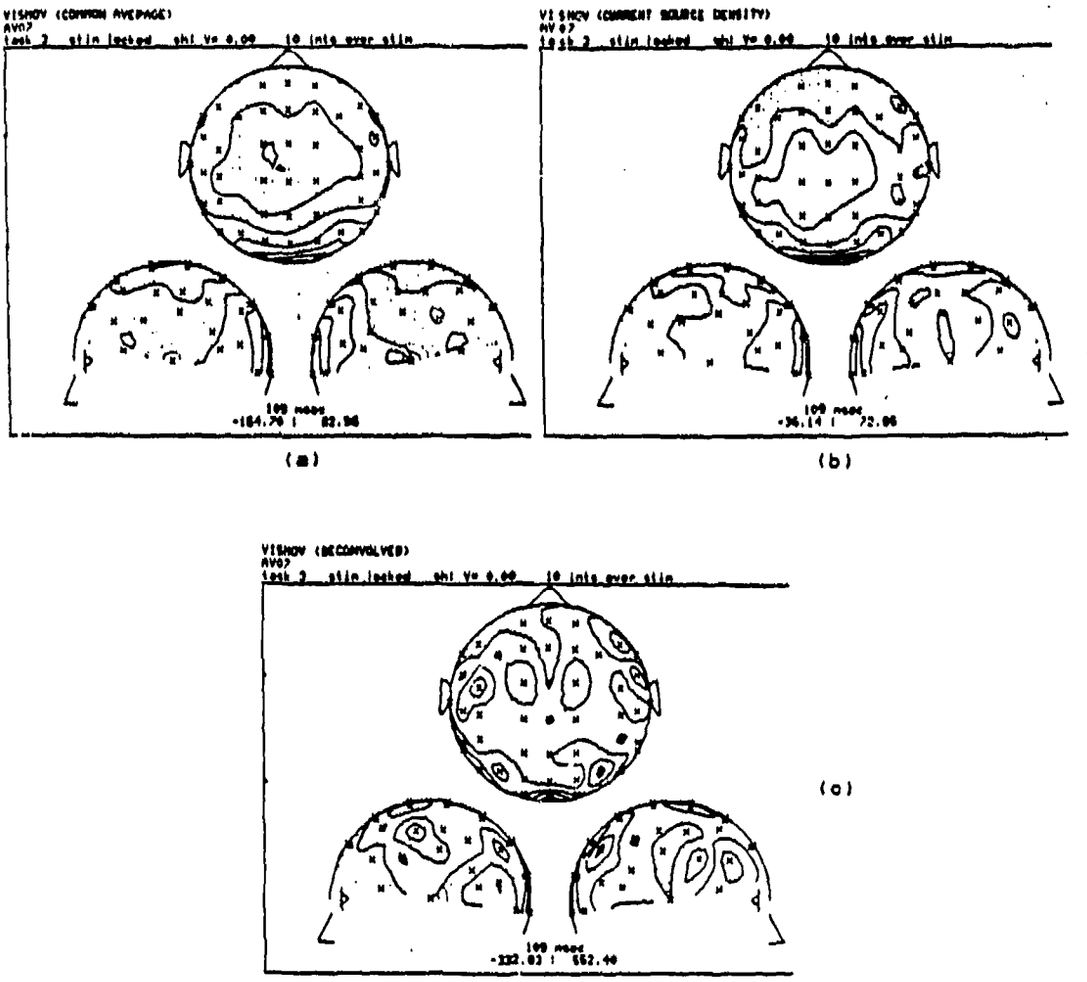

Figure 13

Isofunction contour plots of a visual evoked potential 109 msec after the foveal presentation of a single-digit number. (a) Scalp potential (common average reference). (b) Laplacian Derivation. (c) Dipole strength from deconvolution. In (a) dots are areas of positive potential; in (b) dots are exiting currents; in (c) dots are positive "dipole strengths." In each picture, each contour interval represents a 10% change from its neighbor, the maximum value being at the back of the head.

electrode positions. The responses were also calculated using the original measured coordinates for the electrodes and the 0.75-reduced set for the sources. Use of such reduced sets for the sources corresponds to the situation where one has prior knowledge about the actual sources of the potentials, so that the Helmholtz layer may be assumed to be of approximately zero strength outside a restricted area.

The results of the linear regression of covariance against pointspread function are shown in Table 1. As expected, the common average covariances manifested a large slope and a large ratio of regression variance to residual variance. The Laplacian Derivation caused a considerable reduction in both these quantities, while the deconvolution effected even more reduction.

TABLE 1

INTERELECTRODE COVARIANCE (1)

REGRESSED VERSUS POINT SPREAD FUNCTION

SPATIAL OPERATOR	Slope	Intercept	F-ratio(2)
Common Average	2375.49	-221.51	676.8
Local Laplacian	144.19	-15.53	174.7
Deconvolution	21.95	-4.18	10.6

(1) Interelectrode covariance calculated over stimulus-locked average from 0.5 sec before to 1.0 sec after stimulus.

(2) Ratio of regression to residual variance, df = (1,664).

The response of the three derivations to the progression of simulated source positions is shown in Figure 14 (a,b, and c) for the measured positions, 0.75- and 0.50-reduced positions, respectively. The point-spread function is, of course, the same for each. The resolution advantage of the deconvolution increases as the electrode spacing decreases. Figure 14d shows the deconvolution response for measured electrode positions and 0.75-reduced source positions, as well as the deconvolution response from Figure 14b for comparison. This shows that the resolution of the deconvolution may be usefully improved if one has knowledge of the general location of actual sources within the brain.

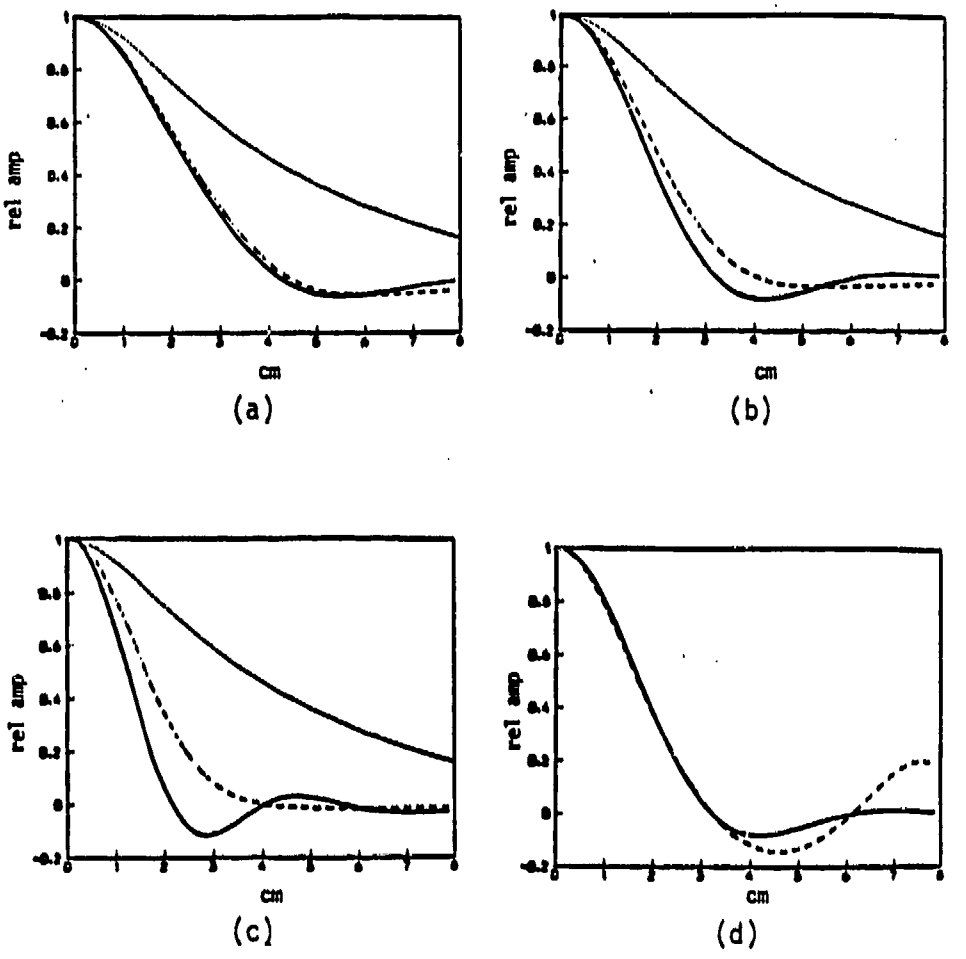

Figure 14

Simulation results showing response of each derivation to radial dipoles as a function of scalp distance. In (a)-(c), the solid line is from the deconvolution, the dashed line is from the Laplacian Derivation, and the dotted line is from the evoked potential. (a) 4-cm spacing of principal electrodes and dipoles. (b) 3-cm spacing of electrodes and dipoles. (c) 2-cm spacing of electrodes and dipoles. Note that the improvement of deconvolution over local Laplacian increases as the electrode spacing decreases. (d) Deconvolution response with 4-cm electrode spacing (solid) compared with response calculated with 4-cm electrode spacing and 3-cm dipole spacing (dashed). Some approximate knowledge of the location of neuronal sources can provide resolution equivalent to having closer spaced electrodes.

The simulation and empirical results suggest that the covariance due to volume conduction is somewhat more reduced by the deconvolution than by the Laplacian Derivation. Although this seems to imply that the deconvolution improves the resolution of brain activity, simultaneous scalp and intracerebral recordings are

required to determine if this is actually so, and many additional recordings need to be analyzed to see if these results replicate. In any case, in the simulations, the advantage of the deconvolution over the Laplacian Derivation increases as the electrode spacing is decreased. The computational requirement of a matrix multiplication on each time point for either method is not prohibitive for use on averages or sets of single trials.

Both deconvolution and source derivation are affected by inhomogeneity in the thicknesses or resistivities of the skull and scalp. If the skull is thinner or less resistive in a particular area, more current will flow through it and the value of Laplacian Derivation or deconvolved activity will be larger than the actual brain activity. For either technique the solution must involve a more accurate and detailed modeling of the tissues. One may measure the scalp and skull thicknesses on each individual, using magnetic resonance images, ultrasound probes, or other methods. Most satisfactory would be the use of a finite-element or finite-difference calculation to model the tissues in detail, including fissures and orifices such as the orbits.

e. *MEG Data Analysis.* A collaboration is underway with the laboratories of Drs. Williamson and Kaufman. The purpose of this effort is to make a gateway for their MEG data into the ADIEEG-IV system so that source modelling using both EEGs and MEGs can be undertaken. (In other research, we have developed adaptive digital filters for removal of environmental noise from MEGs.)

3. *Event-Related Covariances (ERCs)*

A number of steps are currently performed in computing ERCs. Because of the size of the single-trial data sets (up to 500 megabytes for each person), a large on-line disk capacity is required. As already described, the first pass reduces spatial smearing and then selects intervals and trials with task-related information to enhance the signal-to-noise ratio and reduce the amount of data prior to measuring ERCs. The second pass measures ERCs on band-pass-filtered, enhanced (optional), averages from the reduced data set. This second pass requires the following steps:

Compute ERCs: Select digital bandpass filters and intervals for measurement by examining ERPS, amplitude distribution maps and Wigner distributions. Compute multilag crosscovariance functions between all pairwise channel combinations of the enhanced (optional), filtered and decimated averages in each selected analysis window. Use the magnitude of the maximum crosscovariance function and its lag time as features characterizing the ERC [38-41].

Estimate significance of ERCs: Estimating the significance of ERCs requires an estimate of the standard deviation of the "noise" ERC. It is obtained as follows: (1) Random intervals in each single trial of the ensemble are averaged. (2) ERC analysis is performed on a filtered and decimated version of the resulting "noise" averages, yielding a distribution of "noise" ERCs. (3) Multiple comparisons are accounted for with a Duncan procedure.

Graph: The most significant ERCs in each interval are graphed (Fig. 15).

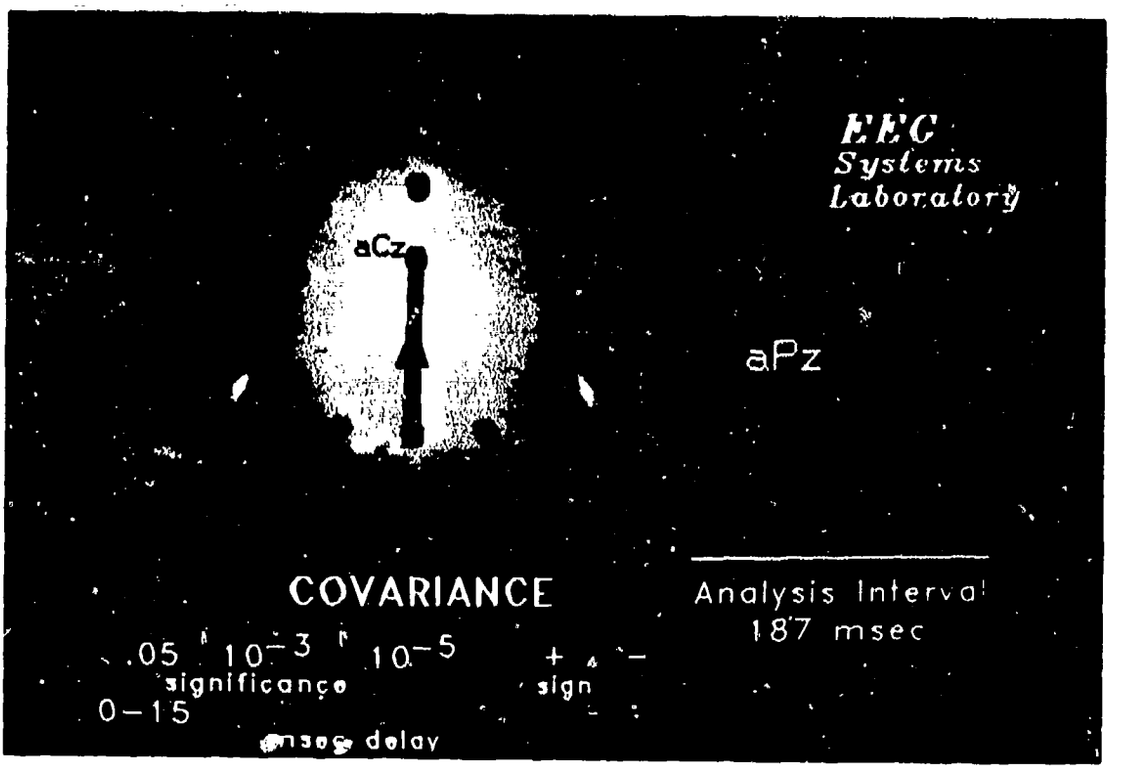

Figure 15

An illustration of a single covariance between the two channels shown at the right. Electrode positions are indicated, and the relationship of a covariance line to the theta-filtered averaged event-related timeseries from the two corresponding electrodes is shown. In all covariance diagrams, the width of a line indicates the significance of covariance between 2 electrodes and its color indicates the magnitude of time delay. When the color of the arrow is the same as the covariance line, the covariance is positive; when the arrow is gray, the covariance is negative. The arrow points from the leading to the lagging channel. (Specific values of significance and delay are given on each diagram.)

Compare ERC maps between conditions: Test the difference in means of significant ERCs between conditions with an ANOVA and post-hoc t-tests. Measure similarity between multivariate ERC maps with an estimate of the correlation between them. Calculate these estimates using a distribution-independent "bootstrap" Monte Carlo procedure [42], which generates an ensemble of correlation values from randomly selected choices of the repeated measures. This will also yield a confidence interval for the estimates.

IV. RECENTLY COMPLETED EXPERIMENTS

A. Bimanual Numeric Visuomotor Experiment [38-40]

This study represented an attempt to non-invasively measure the functional interrelationships of the human brain during simple goal-directed behaviors that required integrated processing by many brain regions. Prior studies using intracerebral electrodes have suggested that there is a consistent morphology and timing of macropotentials from functionally related brain regions [43-45]. Full four sec-long trials spanning prestimulus, stimulus, response execution and feedback intervals were analyzed. Between-channel covariance and time-delay measures were derived from pairs of filtered Laplacian Derivation (LD) average waveforms, enhanced by rejection of trials without event-related signals, in brief intervals spanning evoked potential components. Stimulus- and response-locked covariance patterns were consistent with functional neuroanatomical models of visual stimulus processing and motor execution. Prestimulus patterns predicted subsequent response accuracy by each hand. Feedback patterns also distinguished accurate from inaccurate performance.

1. *Methods*

a. *Subjects.* Seven healthy male adults participated in this study. Mean age of the subject group was 26.7 (range: 21-38 years). All subjects were right-handed and had no history of neurological or psychological abnormality.

b. *Task.* Stimuli, subtending a visual angle under 1.5 degrees, were presented on an amber CRT monitor placed 70 cm from subjects' eyes. Stimuli had a duration of 315 msec and an illumination of 0.5 log fL against a background of -1.5 log fL. A visual cue, slanted to the right or to the left, indicated to subjects to prepare to make a response pressure with the right or left index finger. One second later, the cue was followed by a visual numeric stimulus (number 1-9) indicating the required pressure of the response, from 0.1 kg to 0.9 kg. Subjects were required to respond as quickly and accurately as possible.

Feedback indicating the exact response pressure produced was presented as a two-digit number one second after the peak of the response pressure. The feedback number was underlined if the response pressure did not exceed the required pressure by more than a threshold based on previous performance; the performance threshold was updated on-line after each trial as the average error from the preceding five trials for each hand separately. A random 20% of the trials were no-response trials in which the slant of the stimulus was opposite to that of the cue and no response was to be made. All trials had a duration of about four sec. The inter-trial interval was two sec. Between eight hundred and 1000 trials were performed by each subject.

c. *Recordings.* Twenty-six channels of EEG data were recorded from tin disk scalp electrodes. Electrodes were placed according to an expanded version of the standard Ten-Twenty Electrode System in which additional coronal rows of electrodes were interposed between the original rows. The anterior midline parietal

electrode was used as the reference. EEGs, as well as vertical and horizontal eye-movements and flexor digitori muscle activity from both arms, were digitized at 128 Hz from 0.75 sec before the cue to 1.0 sec after feedback. The bandpass had a 6 dB/octave rolloff below 0.1 Hz and a 24 dB/octave rolloff above 50 Hz. The rolloff below 0.1 Hz was gradual enough to allow sensitivity to ultra-low frequency brain potential components.

The scalp potentials were converted to LDs by approximating the second spatial derivative of the potential field at each electrode. All single-trial EEG data were screened for eye-movement, muscle potential and other artifacts by two independent editors. Contaminated data (20%) were discarded.

d. *Analyses.* Enhanced averages were computed by eliminating individual trials that lacked discernible event-related signals [18]. The criterion for elimination was based on a "noise" set, composed of segments of ongoing EEG for each channel, randomly timed with respect to any stimulus or response event. The distribution of noise segments had statistical properties similar to the distribution of event-related segments. Sets of event-related and "noise" data samples were submitted to a mathematical pattern classification algorithm, which constructed equations to discriminate between the two sets for each channel in a brief time interval (125 or 250 msec). Approximately 60% of the data remained after this procedure. An averaged LD waveform over an entire trial is shown in Figure 16.

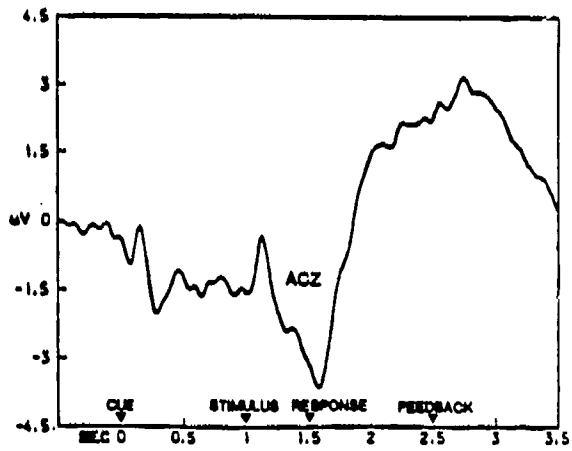

RIGHT MOVE, CUE-LOCKED

7 Hz Filtered Average

Figure 16

A 7-Hz low-pass filtered, Laplacian derivation waveform (aCZ) averaged across seven subjects for a full four-sec cued, bimanual visuomotor task trial. The midline antero-central channel (aCz) is shown.

Intervals used for event-related covariance (ERC) analysis were centered on major event-related potential peaks. Bandpass filter characteristics were determined from Wigner time-frequency distributions of the enhanced average [19]. Covariances were computed between each of the 120 pairwise combinations of the 16 channels in intervals from 500 msec before cue to 1000 sec after the feedback.

i. *Pre-stimulus ERCs:* Data sets were separated into trials in which subsequent performance was either accurate or inaccurate. Accurate and inaccurate performance trials were those in which the error (deviation from required finger pressure) was less than or greater than, respectively, the mean error over the entire recording session. Outlying trials on the distribution of performance threshold were eliminated to ensure that accurate and inaccurate data sets did not differ from each other due to learning or transitory changes in arousal. Accurate and inaccurate trials were evenly distributed throughout the recording session.

ERCs were computed from delta-bandpass-filtered (0.01 to 3 Hz) enhanced averages for a brief, 375-msec-wide interval centered on the Contingent Negative Variation (CNV) (687 msec post-cue; 313 msec prestimulus). Covariance functions were computed by lagging one channel of the pair up to +/- 128 msec. The measure of covariance was the maximum absolute value of the covariance function. The statistical significance of each covariance was assessed by reference to a noise distribution computed from the same data. (Significant ERCs were graphed on color three-dimensional perspective model heads and published in [38]).

ii. *Stimulus-, response- and feedback-registered ERCs:* Analyses of the stimulus-, response- and feedback-registered events were performed by computing ERCs from 187-msec-wide intervals centered on the major event-related LD peaks of enhanced, theta-band filtered (4 to 7 Hz) averages, including the N1, P300 and response potentials. Covariance functions were computed for all channel pairs by lagging one channel of the pair up to +/- 64 msec). (Significant ERCs were graphed on color three-dimensional perspective model heads and will be published soon [39,40]. Feedback ERCs were computed separately for accurate and inaccurate trials as described above for the prestimulus ERCs.

2. *Results and Discussion*

a. *Prestimulus interval.* ERC patterns occurring during an interval spanning the CNV differentiated subsequently accurate and inaccurate trials (Fig. 17). Subsequently accurate performance by each hand was characterized by significant ERCs involving electrodes overlying left-frontal and appropriately lateralized central and parietal cortices. Inaccurate performance by the right hand was preceded by a similar pattern but with fewer covariances. Inaccurate performance by the left hand was preceded by a complex, spatially diffuse ERC pattern. ERC patterns of subsequently accurate and inaccurate performance for both hands differed significantly whereas CNV amplitudes (Fig. 18), *per se*, did not.

Figure 17

View of the most significant ($p<.05$), between-channel ERC patterns from an interval 500 to 875 msec after the cue for subsequently accurate and inaccurate left-hand (A) and right-hand (B) performance by seven right-handed subjects. The thickness of a line is proportional to its significance (from .05 to .005). Line color indicates the sign of the covariance (violet = positive; blue = negative). Covariances involving left-frontal and appropriately lateralized central and parietal electrode sites are prominent in patterns for subsequently accurate performance of both hands. Magnitude and number of covariances are greater preceding subsequently left-hand inaccurate performance; fewer and weaker covariances characterize subsequently inaccurate right-hand performance.

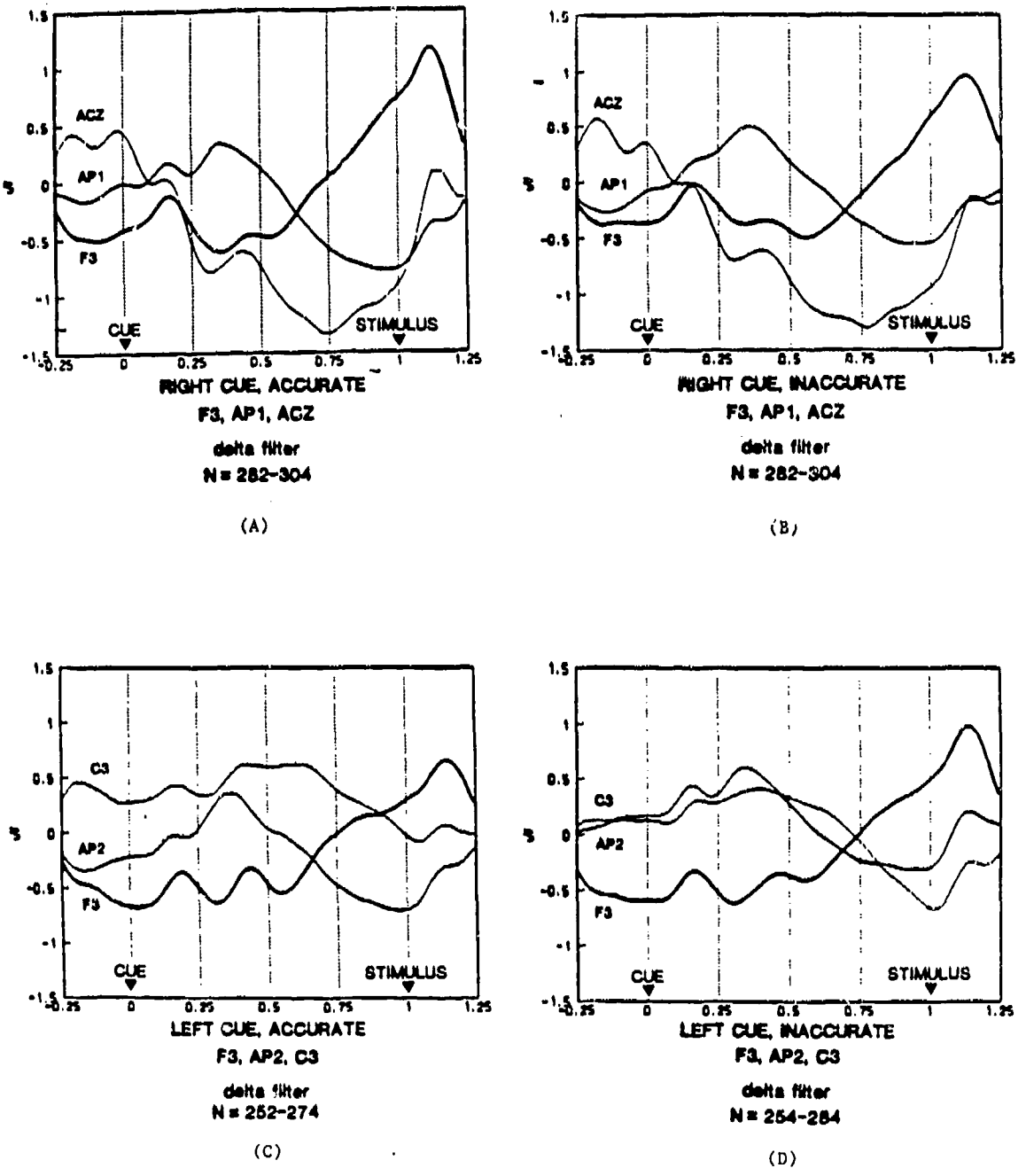

Figure 18

Delta-filtered Laplacian Derivation waveforms showing the CNV in the cue-to-stimulus period from the left-frontal (F3), anterior midline central (aCZ) and left antero-parietal (aP1) sites for right-hand accurate (A) and inaccurate (B) performance, and from left-frontal, midline antero-central and right antero-parietal (aP2) sites for left-hand accurate (C) and inaccurate performance (D). The mean amplitudes of the late CNV, from low-pass filtered (below 3 Hz) averages of seven subjects, did not differ significantly between accuracy conditions for either hand [38].

These findings are particularly interesting in light of unresolved issues concerning the relationship between the CNV and anticipatory and preparatory processes [46,47]. One important issue has been whether this slow potential solely reflects motor preparation or whether a cognitive component related to an expected stimulus is also involved. In addition, among attempts to relate CNV to the quality of subsequent performance, even the most recent have had negative or mixed results (e.g., [48]) Our findings indicate that the CNV is a multi-faceted process with components that function synergistically to achieve subsequently accurate performance.

We speculate that the prestimulus ERC patterns reveal the existence of a preparatory neural set that involves distinctive cognitive (frontal), integrative-motor and lateralized somesthetic-motor components. The involvement of the left-frontal site is consistent with clinical findings that preparatory sets are synthesized and integrated in prefrontal cortical areas (reviewed in [49]) and with experimental and clinical evidence indicating involvement of the left dorsolateral prefrontal cortex in delayed response tasks. A midline antero-central integrative motor component is consistent with known involvement of premotor and supplementary motor areas in initiating motor responses [50,51]. The finding of an appropriately lateralized central and parietal component is consistent with evidence from primates and humans for neuronal firing in motor and somatosensory cortices prior to motor responses (e.g., [52,53]).

The fact that stronger ERC patterns were found for subsequently inaccurate left-hand than for inaccurate right-hand performance, particularly for sites overlying motor areas, may indicate that a "stronger" preparatory set is required for left-hand performance by strongly right-handed subjects. In a study of rhesus monkeys, Johnson [53] reported that slow potential activity for the initiation of voluntary movement begins earlier, and is present over medial prefrontal cortex bilaterally, for movement of a non-preferred hand relative to a preferred hand. The generally diffuse ERC patterns for subsequently inaccurate left-hand performance compared with the right may also suggest that inaccurate left-hand performance results from erroneous or confounded preparatory sets.

b. *Stimulus interval.* Response and no-response conditions for right- and left-slanted stimuli were examined in early and late poststimulus intervals. For the interval on the N1 peak, ERC patterns (Fig. 19) were differentiated according to the direction of stimulus slant, but not to response condition. The right parietal site was involved in patterns for both right- and left-slanted stimuli, perhaps reflecting the importance of that region in attentional tasks [54]. An additional parietal component, ipsilateral to the stimulus slant, appeared to represent an obliquely oriented contralateral occipital generator that projected to the opposite hemisphere.

ERCs in the interval centered at 312 msec on the P300 peak differed substantially between response conditions (Fig. 20), but no longer between stimulus conditions. The midline antero-central site (aCZ) was prominently involved in ERC patterns for the no-response condition in this interval, possibly reflecting involvement of the underlying supplementary motor and premotor cortices in motor inhibition.

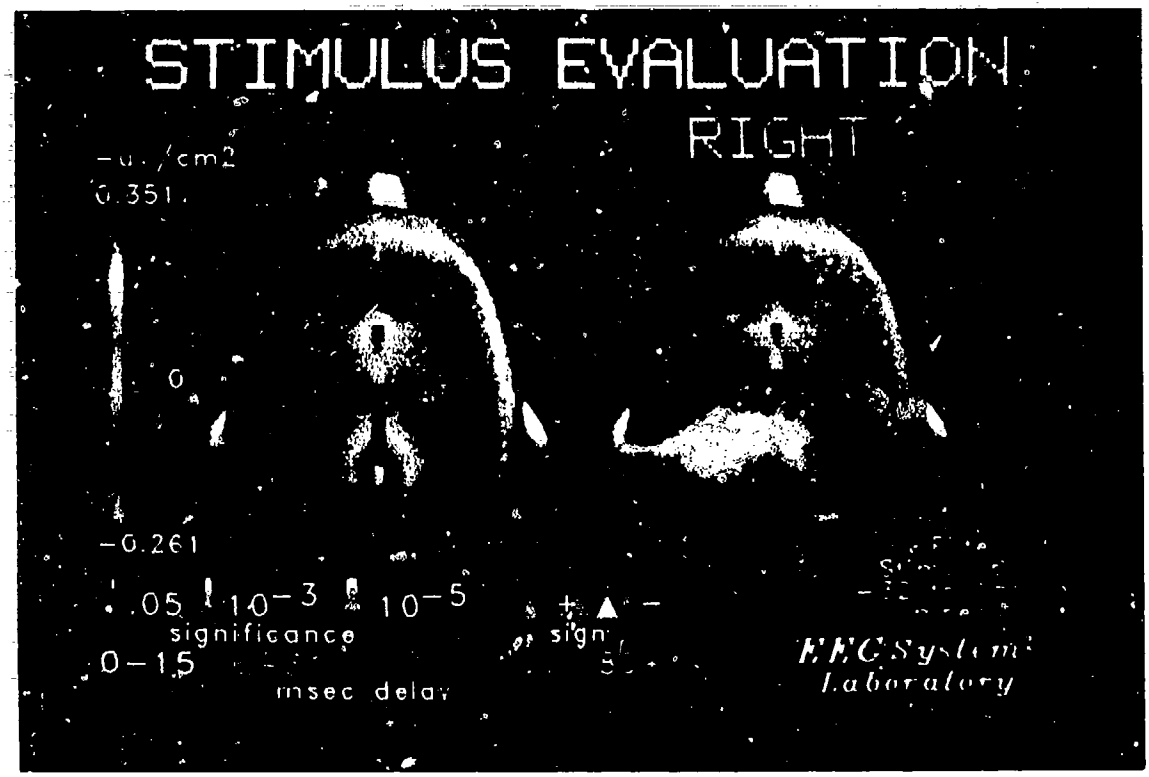

Figure 19

View of the most significant (top standard deviation) ERC patterns (colored lines), looking down at the top of the head, from the stimulus-locked waveform of the response condition, superimposed on colored maps of N1 wave amplitude. The event-related covariances were measured during a 187-msec-wide interval, centered 62 msec after left and right stimulus onset, from theta-band filtered, 7-subject averages. The thickness of a covariance line is proportional to the negative log of its significance (from .05 to .00005). The color scale at the left, representing wave amplitude, covers the range from the minimal to maximal values of the two maps. For both left- and right-handed conditions, there is a maximum of wave amplitude occipitally and a minimum at the antero-central site. Common covariances for both left- and right-hand conditions exist between midline posterior parietal (Pz) and antero-parietal (aPz), and between midline antero-parietal and antero-central (aCz) sites. Additional covariances for the right-hand condition, involving the right parietal (P4) site, reflect the lateralization of the N1 peak at parietal sites.

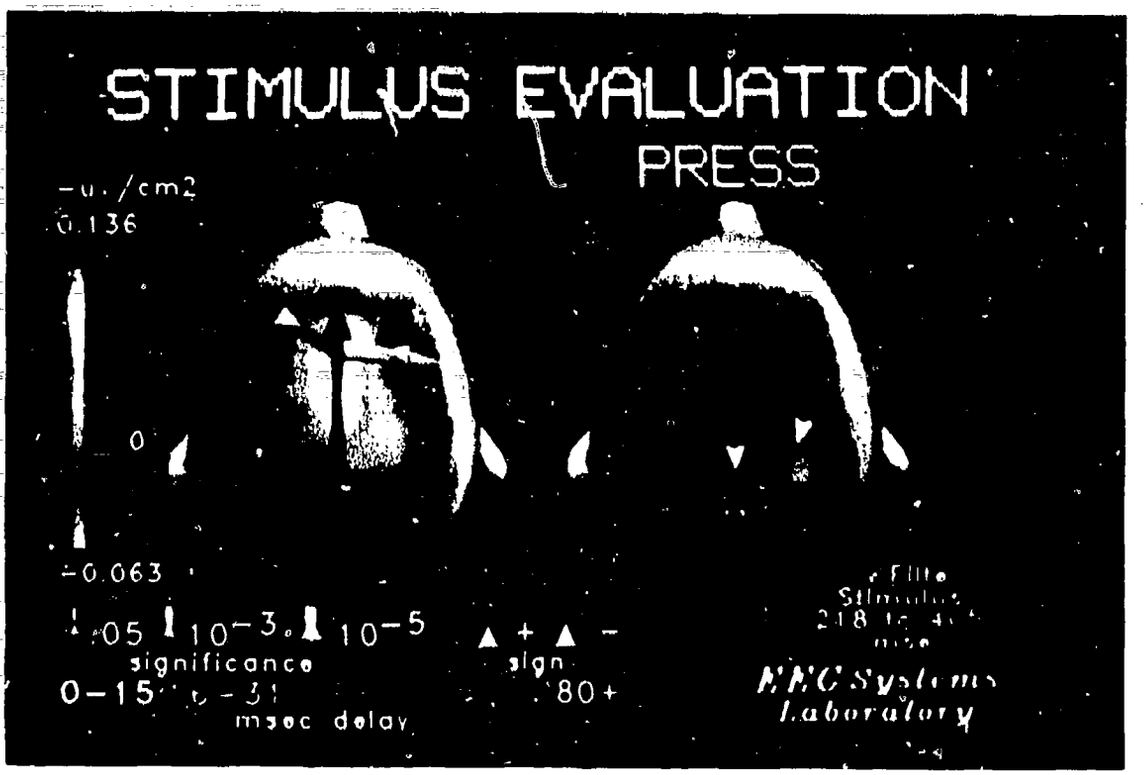

Figure 20

View of the most significant (top standard deviation), P300 ERC patterns (colored lines), looking down at the top of the head, superimposed on colored maps of integrated P300 amplitude. Measurements are from an interval 218 to 405 msec after right-cue stimulus onset, for response ("PRESS" for pressure) and no-response ("NO PRESS" for no pressure) conditions, on the P300 peak of theta-band filtered, 7-subject averages. The midline parietal site (Pz) is central to the pattern for the response condition, and the midline antero-central site (aCz) is central for the infrequent no-response condition. Pz lags most other sites in the response condition, while aCz lags in no-response.

c. *Response interval.* Differences between right- and left-hand response conditions were examined in intervals before and after response onset. At the peak of the finger pressure (62 msec after response onset; Fig. 21), ERC patterns were appropriately contralateral to the hand used (Fig. 22). The midline antero-central site was prominent in all patterns. The sign of the ERCs of this site with posterior, left-central (C3) and antero-parietal (aP1) sites for right movement, and right-central (C4) and antero-parietal (aP2) sites for left movement, was opposite to that with anterior sites, reflecting the transition from an anterior current sink to a posterior current source. The lack of significant ERCs between lateral central and antero-parietal sites suggests the existence of separate generators on either side of the central sulcus covarying with a third generator under the midline antero-central site, possibly in supplementary motor cortex.

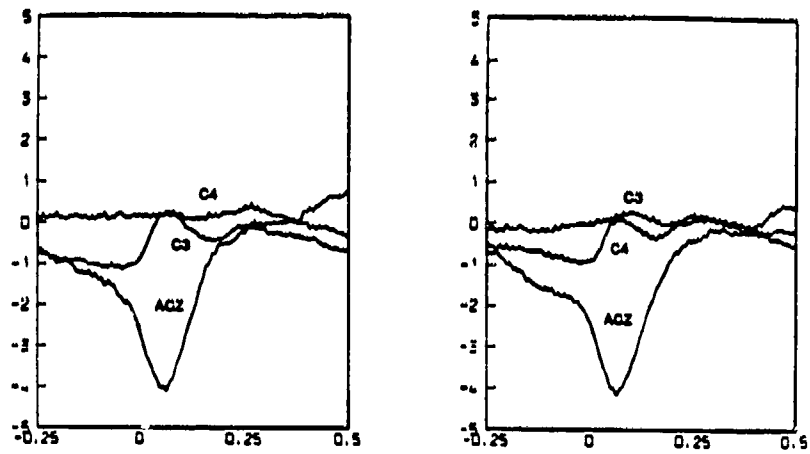

Figure 21

Response-locked, Laplacian Derivation waveforms for right-hand (A) and left-hand (B) responses from midline antero-central (aCZ), left- and right-central (C3, C4) sites averaged across seven subjects. Emerging "equivalent current" is up.

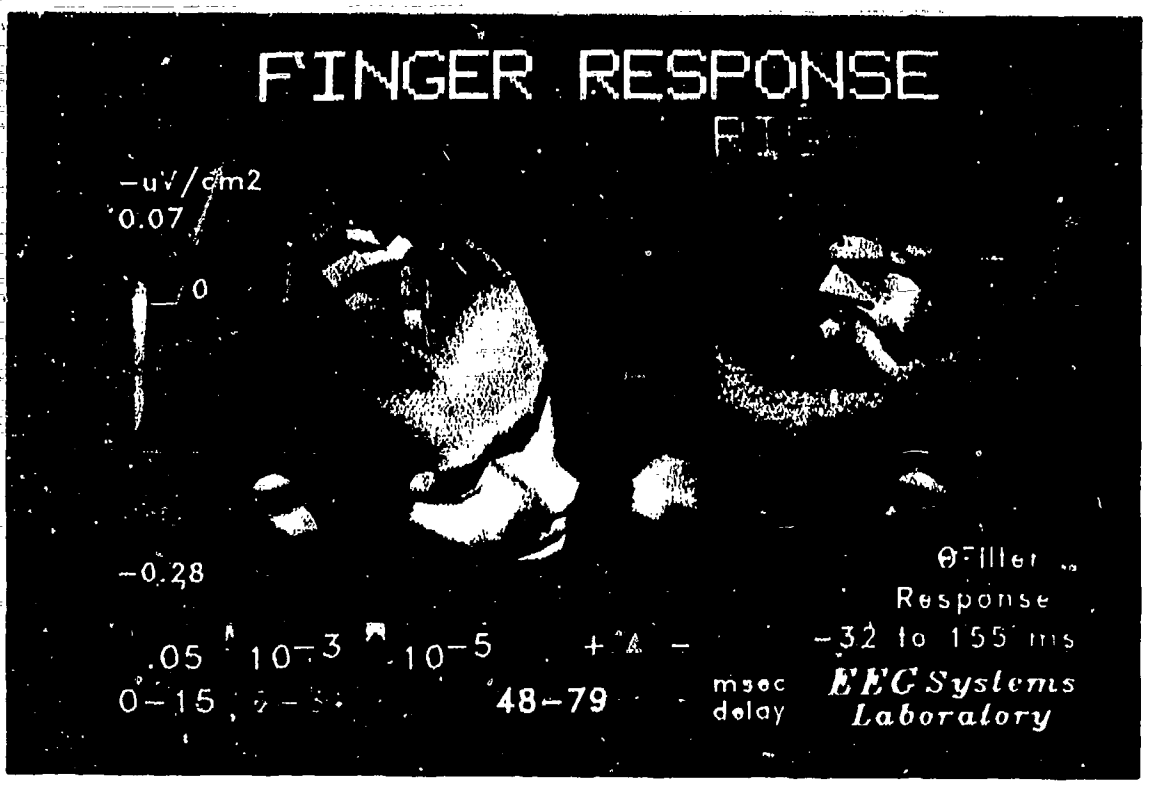

Figure 22

View of the most significant, ERC patterns from the wave at the peak of the finger response. The motor-related wave was measured during a 187-msec interval centered on the peak of the left-hand and right-hand index finger pressures from theta-band filtered, seven-subject averages. The thickness of a line is proportional to its significance (from .05 to .00005). Line color indicates the time delay (lag time of maximum covariance), and the arrow points from the leading to the lagging channel. Colored arrows or boxes indicate positive covariances, while tan arrows or boxes indicate negative covariances.

d. *Feedback interval.* Distinct ERC patterns associated with visual feedback about accuracy of response performance were most clearly defined in the 187-msec-wide interval, centered 375 msec post-feedback (Fig. 23). Prior to this interval (in intervals centered 125 msec and 250 msec post-feedback, for example), ERCs for both hands, irrespective of accuracy, involved almost exclusively the posterior, central, and antero-central midline channels. Beginning with the interval centered at 375 msec, a pattern involving ERCs from midline occipital and parietal to midline antero-central and right-frontal sites was common to both accurate and inaccurate right- and left-hand responses. When responses were inaccurate, the feedback pattern additionally included the left antero-central site for the right hand and the left-frontal site for the left hand. Therefore, while feedback to accurate performance involved midline sites and sites overlying the right frontal cortex, feedback to inaccurate performance was characterized by a more symmetric ERC pattern involving sites overlying frontal, central and parietal areas bilaterally. These patterns were not apparent in topographic maps of the average ERPs.

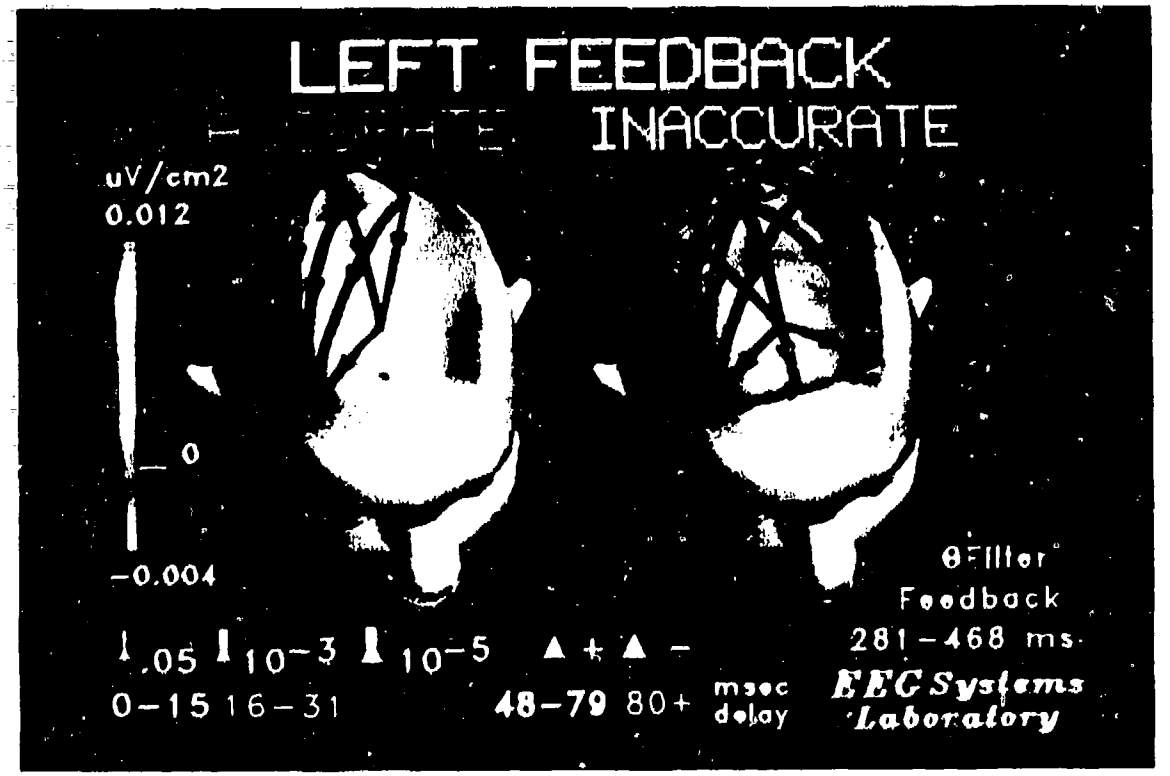

Figure 23

View of the most significant (top two standard deviations), ERC patterns (colored lines), looking down at the top of the head, for feedback to accurate and inaccurate performance by the left hand (A and B)and right hand (C and D). ERC patterns are superimposed on color maps of wave amplitude. The thickness of a covariance line is proportional to the negative log of its significance (from .05 to .00005). The color scale at the left of each picture, representing wave amplitude, covers the range from the minimal to maximal values of the two maps. Both the covariances and the amplitude maps are derived from a 187-msec-wide interval, centered at 375 msec after feedback onset, on theta-band-filtered 7-subject averaged waveforms. Patterns were similar between hands and conditions in an early interval centered at 125 msec, and began to differ in the interval centered at 287 msec which spanned part of the early P300. For the interval centered at 375 msec shown in the figure, the patterns for feedback to accurate performance involve the right frontal and antero-central sites, but not the left. The patterns for feedback to inaccurate performance additionally involve the left frontal and antero-central sites, and the right parietal site. These sites may reflect additional attention necessary to improve performance on subsequent trials.

Previous evoked potential studies of feedback about performance accuracy have suggested that evaluation of feedback information may be a serial process [55,56]. It has been suggested that an early P300 is associated with the identification or classification of feedback and that a later positive wave is associated with the subsequent utilization of that feedback information. Our results provide further information about the dynamic temporal and spatial processes related to feedback about performance accuracy. Involvement of the midline antero-central site (overlying the supplementary motor area) following feedback to both accurate and inaccurate performance may reflect "motor recalibration" consequent to feedback information. The involvement of frontal sites may reflect feedback-specific "updating" and behavioral verification. These interpretations are consistent with experimental and clinical evidence suggesting that frontal and supplementary motor cortices are involved in planning and sequencing voluntary behavior [49]. Involvement of the left-frontal site specifically for feedback about inaccurate performance is particularly interesting because its involvement is also a distinguishing feature of the preparation period preceding accurate performance.

In conclusion, the measurement of event-related, between-channel covariances provides insights into the spatiotemporal characteristics of preparation, stimulus processing, response execution and processing of feedback information in a difficult visuomotor task. Taken together, the ERC patterns appear to reflect the co-ordination of specific neural regions. Although the origin of these patterns is not yet clearly understood, their consistency with previous neuroanatomical models suggests that they primarily reflect cortical activity. The focal, spatially separated patterns tend to rule out an explanation based solely in terms of volume-conducted activity from one or two distant subcortical or cortical generators. In view of the striking findings, determining the actual source of these patterns is a compelling issue.

B. Fatigue Experiment

1. *Overview*

Impaired behavior consequent to prolonged mental work is commonly attributed to the effects of fatigue on higher cognitive functions rather than to changes in rote perceptuomotor or motor functions. A deeper understanding of these effects awaits better knowledge of the underlying neurophysiological mechanisms. Towards this end, event-related, spatiotemporal neuroelectric patterns of five U.S. Air Force test pilots performing a high-load visuomotor monitoring task while they were alert, becoming fatigued, and fully fatigued. These results suggest that the effects of mental fatigue are not only evident in spatially- and temporally-specific neuroelectric patterns prior to overt signals of behavioral deterioration, but that cortical networks underlying certain higher cognitive functions are selectively altered during the incipient stages of fatigue while those involved in visual stimulus processing are relatively unaffected. With further research, it may be possible to design on-line devices for predicting "transient cognitive lapses" and performance decrements resulting from operational fatigue.

2. *Introduction*

It is well known that higher cognitive functions are more affected by fatigue due to prolonged, difficult mental work, than are rote perceptuomotor or motor functions. Although psychological theories have attempted to explain these changes, numerous reports of tragic accidents caused by fatigued pilots and operators of other complex equipment clearly demonstrate the need for a better understanding of these phenomena. Here we report a study of event-related, spatiotemporal neuroelectric patterns associated with visual stimulus processing and response inhibition: five U.S. Air Force test pilots performed a high-load visuomotor memory task while alert, becoming fatigued, and fully fatigued.

The study emerged from the collaboration of researchers from several institutions: (1) The USAF School of Aerospace Medicine, San Antonio (James Miller); (2) Systems Technology Inc., Hawthorne, California (Henry Jex and James Smith); (3) Washington University, St. Louis (John Stern); and (4) The EEG Systems Laboratory. A paradigm was developed that included several cognitive and perceptuomotor tasks requiring varying degrees of attention, working memory, and skill. Thirty-three or 51 scalp EEG, two eye-movement, and several other physiological channels of data were recorded from each of the five test pilots as they performed the task battery.

3. *Methods*

a. *Requirements.* The present experiment took into account certain criteria that must be met in order to isolate the effects of operational fatigue on performance to ensure that the results would have a modicum of construct and face validity for real-life situations, such as piloting an aircraft. These criteria included: (1) tasks that are taxing in an alert state, yet manageable in a fatigued state; (2) tasks meeting constraints imposed by neurophysiological recordings and analysis, including minimal eye- and head-movements, and isolation of stimulus, response, and cognitive variables [3,4,57,58]; (3) experimental paradigms controlled for initial task learning and automatization of performance; and (4) recording sessions that extend from well-practiced, alert performance to fatigued and decremented performance due to extended time-on-task.

b. *Experimental Protocol.* The experiment was conducted over the course of four days. Pilots learned and performed a battery of tasks for about 6 hours on the first day until their performance stablized (Session 1). They returned to the laboratory the following morning, were prepared for recording, and began performing the tasks at about 1:30 PM (Session 2). After a dinner break at about 8:00 PM, they resumed task performance for an additional 6-8 hours (Session 3) until they could no longer continue, or usable EEG data could no longer be recorded because of excessive eye movements or head nodding and drooping.

Recordings were made in an acoustically dampened, air-conditioned chamber. Room temperature, lighting, and seating position were adjusted as necessary.

c. *Task Battery.* The total task battery consisted of five tasks: (1) Visuomotor Monitoring Task, null memory condition; (2) Visuomotor Memory Task, memory

load condition (called VMMT in this report); (3) Auditory Monitoring Memory (AUM) Task; (4) Sub-critical Tracking; and (5) Critical Tracking [59,60]. The four tasks alternated within experimental units each lasting about two hours. The analysis reported here focused exclusively on the difficult VMMT. Results for the other tasks will be described elsewhere.

The VMMT constituted about 40% of each two-hour unit. It was designed to allow for precise control of stimulus parameters, motor activity including eye movements, and cognitive processes. This was done by combining a numeric judgment task used previously [6,38] with a memory element based on the "delayed digit cancelling task." It required that subjects hold a stimulus number in memory, despite numeric distractors, to produce a precise finger pressure corresponding to that number two trials later (Fig. 24). Each trial began with a warning: the disappearance of the letter X from the video screen. This was followed 0.75 second later by the appearance of a single-digit stimulus number to be remembered. Subjects were then required to respond to the stimulus number presented two trials back. This response consisted of a flexion of the right index finger on an isometric transducer with a pressure of 0.1 to 0.9 kg. One second after the peak of the response, a two-digit feedback number was presented indicating the applied pressure with a precision of 0.01 kg. For example, if the stimulus numbers in five successive trials were 8,6,1,9,4, the correct finger-pressure responses would be 0.8 kg to the 1, 0.6 kg to the 9, and 0.1 kg to the 4.

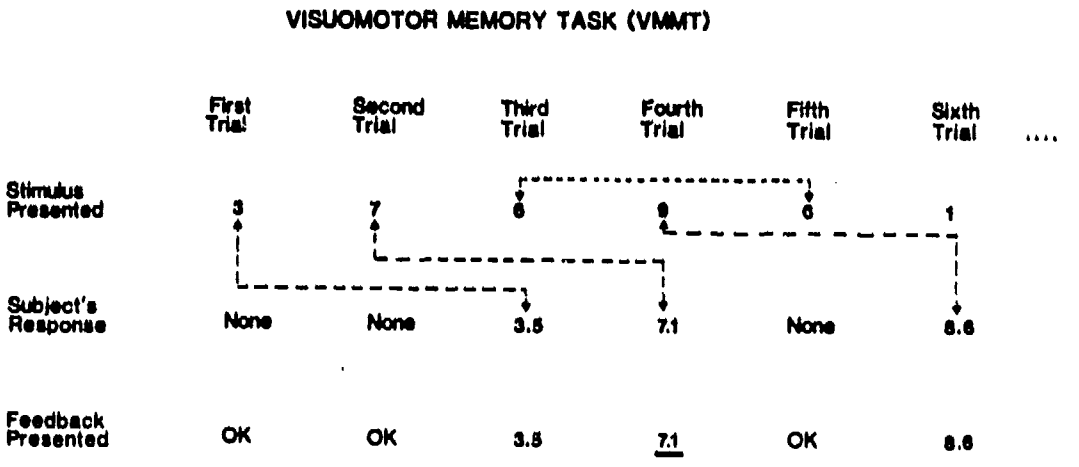

Figure 24

The visuomotor-memory task (VMMT) required subjects to remember, during each trial, the stimulus number from two trials back to produce a precise right index finger pressure. Each trial consisted of a warning (disappearance of the letter X from the video screen — not shown), followed 0.75 second later by presentation of a single-digit visual stimulus to be remembered, followed by the subject's finger-pressure response to the stimulus number presented two trials back, followed 1 second after the peak of the response by presentation of a 2-digit feedback number indicating the accuracy of the response. If the subject's response was highly accurate, the feedback number was underlined. To further increase the task difficulty, subjects were required to withhold their response when the current stimulus number was identical to the stimulus two trials back. (No response was required on the first two trials of each block of 50 trials — signified by "OK").

To further increase the task difficulty, subjects were required to withhold their response whenever the current number was identical to the number two trials back. For example, presented with 9,4,9 as the stimulus numbers in three successive trials, the subject was to inhibit his finger response to the second nine. These no-response trials comprised a random 20% of the trials.

Stimuli were presented for 325 msec on a Videographics-II amber CRT monitor 70 cm from the subject. Stimuli subtended a visual angle under 1.5 degrees, with an illumination of 0.5 log fL against a background of -1.5 log fL. The stimulus and feedback numbers were given in "response units", 10 times the target and actual pressures (in kg), respectively. The feedback number was underlined if the response was a "win." A "win" response was based on an adaptive error tolerance, computed as the geometric average of the error (distance from the required response pressure) on the previous five trials [6]. This adaptive error tolerance served to equalize subjective task difficulty across the session, to indicate the current performance trend, and to increase the difficulty of earning "bonus points" during episodes of improving performance. At the end of each block of 50 trials, subjects were given a block report indicating their performance accuracy, number of time-outs and false responses, and bonus points earned.

There was 0.75 sec from the warning (X off) to stimulus onset, an average of 0.54 sec to response onset, and average of 0.07 sec to response peak, 1.00 sec to feedback onset, then 1.25 sec to the end of trial (X on), and then 1.80 sec inter-trial interval. Thus, the time from one warning to the next was 5.4 sec, and from one stimulus to its response two trials later was 11.4 sec. This pace was fast enough to minimize rehearsal, while still allowing the well-practiced subjects to maintain the numbers in working memory [61].

During pilot studies, subjects commonly reported that, after practicing the task, they developed an accurate "sense" for the 2-back number. Several of the subjects also developed faster reaction times in the memory task than in the comparable non-memory task, yet exhibited no deficiency in detecting stimulus matches on the no-response trials. This suggested a priming of the motor system (since the required two-back number was known), with the ability to abort this preparatory facilitation upon recognition of a two-back match.

d. *Physiological and Anatomical Recording Methods.* Fifty-one EEG channels were recorded for three of the five subjects with a custom nylon mesh cap. Recordings of the other two subjects were made with a reduced 33-channel montage. All signals were amplified by a 64-channel Bioelectric Systems Model AS-64P with .016 to 50 Hz passband, monitored on three 8-channel and two 16-channel polygraphs, and digitized to 11 bits at 128 Hz. Vertical and horizontal eye movements (VEO, HEO), flexor digitorus muscle (EMG), cardiac rate (EKG), respiration, and left mastoid were recorded from all subjects. For all five subjects, recordings were made with the following set of 33 scalp channels referenced to the right mastoid: left and right antero-frontal (aF1, aF2), left and right inferior frontal (F7, F8), left and right superior frontal (F3, F4), midline frontal (Fz), left and right antero-central (aC3, aC4), midline antero-central (aCz), left and right inferior temporal (T5, T6), left and right superior temporal (T3, T4), left and right central (C3, C4), midline central (Cz), left and right inferior antero-parietal (aP3, aP4), left

and right superior antero-parietal (aP1, aP2), left and right mid-parietal (P3, P4), midline mid-parietal (Pz), left and right postero-parietal (pP1, pP2), midline occipital (OZ).

Before and after a recording session, the position of each electrode was measured using a 3-D digitizer. A general ellipsoid surface was fitted to the set of digitized positions, thus defining the outside shape of the head. For the three subjects with 51-channel recordings, full sets of 3-axis MR image brain scans were made at 1-cm intervals over the whole volume of the head. After scaling, translation and registration with the EEG electrode positions, the MRIs allowed correlation of electrode positions and major cortical landmarks [8,62].

e. *Reduction of Volume Conduction Blurring of EEGs.* An optimal least-squares estimate of the Laplacian operator was applied to the EEGs to eliminate dependence on the recording reference electrode and to compensate for the blurring of brain potentials due to their transmission through the skull and scalp [8,10]. Because estimating the Laplacian at peripheral electrodes is problematic, they were eliminated from the analysis. This left 18 remaining non-peripheral electrodes common to all five subjects.

f. *Formation of Data Sets.* Polygraph records were edited off-line by two independent raters to eliminate trials with evidence of eye movement, muscle or instrumental artifacts. Trials in which response pressures were not unimodal or in which reaction time exceeded 1500 msec were discarded. The first two trials of each block, and no-response trials in which the subject responded, were also eliminated.

VMMT trials were divided into "alertness" (that is, "Alert," "Incipient Fatigue" and "Full Fatigue") conditions. Behavioral variables (including adaptive error tolerance, response error, reaction time, number of time-outs on response trials, and number of responses on trials) were graphed across trials for each session. The "Alert" data set consisted of trials from Session 2 that had optimal performance as evidenced by: (1) low adaptive error tolerance on response trials; (2) zero time-outs on response trials; and (3) zero false responses on response-inhibition trials. Trials from early portions of Session 3 with little or no performance decrement formed the "Incipient Fatigue" data set. Trials occurring later in Session 3 formed the "Full Fatigue" data set.

We decided to select only the most accurate trials from the Alert data set, and trials with comparable accuracy from the Incipient Fatigue and Full Fatigue data sets, because we previously found clearcut neuroelectric patterns specific to accurate performance [38,40]. Selection of the most accurate trials was done for each subject individually, with the ADISORT program. Using this interactive program, the three trial sets were divided into subsets with relatively accurate or inaccurate responses, in which the error was less or greater than, respectively, the mean error of the Alert condition trials. Then the least accurate trials of the accurate Incipient Fatigue and Full Fatigue subsets (roughly 2-4% of the trials of each) were discarded, making performance equivalent ($p>0.2$) between each of the Fatigue accurate subsets and the Alert accurate subset.

The resulting performance equivalence allowed for rigorous testing of the

neuroelectric signs of incipient fatigue while controlling for effects due to small variations in performance. Trials for Alert, Incipient Fatigue, and Full Fatigue conditions were performed from about 1:30 PM to 8:00 PM, from about 8:30 PM to 10:30 PM, and from about 11:30 PM to 1:30 AM, respectively. According to a 7-point U.S. Air Force School of Aerospace Medicine Subjective Fatigue Rating Scale (with 1 corresponding to maximal alertness and 7 to complete exhaustion), the average ratings of the five pilots for the three conditions were 3.44 +/- 1.85, 5.25 +/- 1.42 and 6.23 +/- 0.65.

g. *Averaged LDs.* Grand-average (over the five pilots) LDs from event-related potentials were computed time-locked to the stimulus. Because each pair of data sets was balanced behaviorally, we could subtract the LDs of the Incipient Fatigue set from those of the Alert set, and of the Full Fatigue set from those of the Incipient Fatigue, to determine the task-related neuroelectric effects associated with fatigue, unconfounded by trends of declining performance. Use of the subtraction technique required that several conditions be met, including the above-mentioned experimental controls, as well as the absence of large shifts in the latency of peaks between the two conditions. By subtracting the LDs of one set from the other, differences between them were highlighted and common elements were cancelled out.

h. *Event-Related Covariances (ERCs).* Spatiotemporal neurophysiological patterns were quantified by measuring the event-related covariance (similarity of amplitude-weighted waveshape and between-channel timing) between averaged waveforms from all pairwise combinations of electrodes. This analysis was performed with the methods of Section IIIB [see also 5-8,38-41,62,63].

Changes from Alert to Incipient and from Incipient to Full Fatigue conditions were assessed by computing ERCs across brief intervals of the appropriate five-subject grand-averaged, bandpass-filtered, subtraction LDs. ERCs were measured between all 153 pairwise combinations. The first ERC interval, applied to the delta-bandpass-filtered (0.01 to 3 Hz) LD of the finger-pressure response trials, was 500 msec wide and was centered on the CNV (312 msec before presentation of the numeric stimulus). The next two ERC intervals were 187 msec wide and were centered on the theta-bandpass-filtered (4 to 7 Hz) N125 and P380 peaks (of the response and response-inhibition averages, respectively) elicited by the numeric stimulus.

ERC features were the maximum absolute value of the timeseries crosscovariance function formed when the covariance function was computed to 16 lags (+/-128 msec) for the delta-band-filtered prestimulus interval and 8 lags (+/-64 msec) for the theta-band-filtered poststimulus intervals. The significance of the ERC magnitude was determined by reference to the standard deviation of an ERC "noise" distribution obtained from the set of alert trials. Multiple comparisons were accounted for using a Duncan procedure. All significant ERCs in each interval were graphed on 3-D perspective models of the head, or on sagittal or horizontal views of the MR scans. The lag time of the maximum covariance was not examined for ERCs because of the difficulty of interpreting the delay between two subtraction LDs.

4. *Results*

a. *Behavioral.* In the original data sets, performance declined significantly over the three conditions ($F=12.5$, $df=2,12$, $p<.001$) (Fig. 25). Scheffe post-hoc tests revealed that performance did not decline significantly from Alert (1.17 unit departure from target number) to Incipient (1.51) conditions, but did decline significantly from Incipient to Full Fatigue (2.08) conditions ($F=12.28$, $df=2,12$, $p<0.001$). The number of false responses during no-response trials, as well as the number of time-outs on response trials, also tended to increase across alertness conditions. The increase in the number of false responses was significant ($F=17.5$, $df=2,12$, $p<0.001$), and Scheffe post-hoc tests revealed that the number of false responses increased between Alert and Full Fatigue conditions ($F=15.96$, $df=2,12$, $p<0.001$), and between Incipient Fatigue and Full Fatigue conditions ($F=9.42$, $df=2,12$, $p<0.003$). Although the number of time-outs tended to increase with increasing fatigue for all subjects, the effect was not significant.

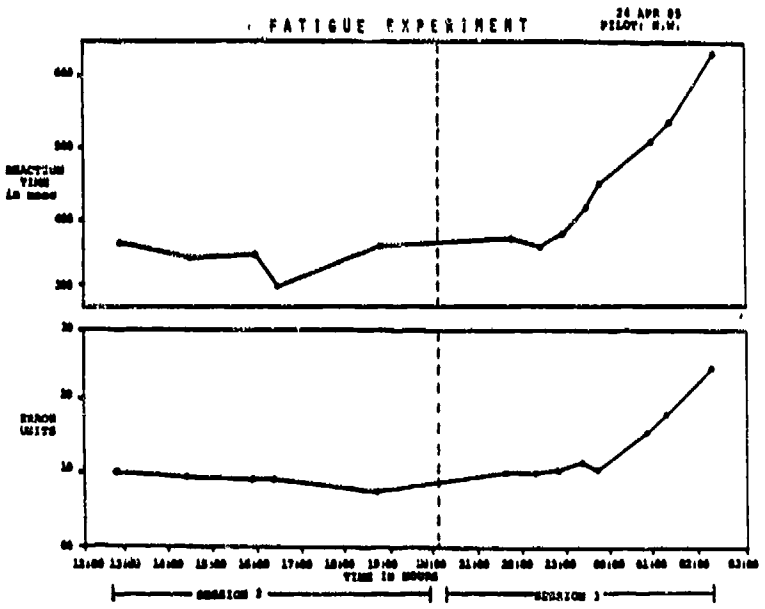

Figure 25

Performance degradation shown as participants fatigued. Reaction time and error both increased with time-on-task. The degradation accelerated substantially in this participant after about 10 hours of performance. Alert trials were taken from the first seven hours in Session 2 when performance had not yet degraded; Incipient Fatigue trials from the following two hours when performance was just beginning to degrade (end of Session 2 and beginning of Session 3); and Full Fatiuge trials from the last several hours of Session 3 when performance was most degraded.

b. *Neurophysiological.* The root-mean-square amplitude of the CNV, over the 500-msec prestimulus interval (Fig. 26A), did not differ across alertness conditions. There was a marked decrease at one channel (midline central), however, from Alert (5.2 μV/ cm^2) to Incipient Fatigue (1.7 μV/ cm^2). Yet at another channel (left superior antero-parietal) there was a slight increase from Alert (2.1 μV/ cm^2) to Incipient Fatigue (2.8 μV/ cm^2).

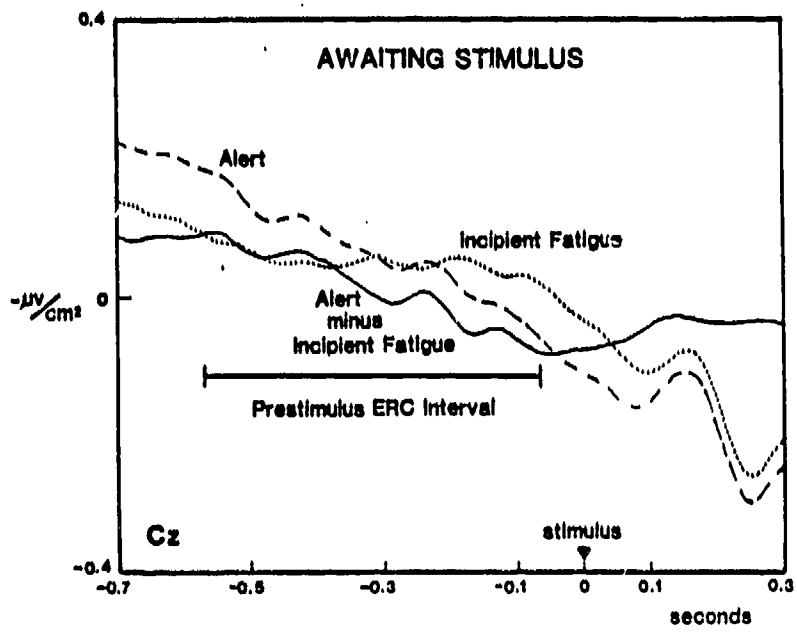

Figure 26A

Grand-average (over five subjects), LD waveforms of the midline central (Cz) electrode during the visuomotor-memory task for Alert (594 trials) (dashed line), Incipient Fatigue (517 trials) (dotted line), and for Alert-minus-Incipient-Fatigue (solid line). The rms amplitude from 562 to 62 msec before the stimulus did not significantly differ between Alert and Incipient Fatigue conditions.

A number of significant Alert-minus-Incipient-Fatigue ERCs were found during the same prestimulus interval. Four of the five significant ERCs involved the midline central electrode (Fig. 26B). ERCs between midline central and left mid-parietal, and left superior antero-parietal electrodes were strongest, with additional significant covariances involving right superior antero- and postero-parietal electrodes. The values of the five significant ERCs were: -44 (midline central to left mid-parietal), -40 (midline central to left superior antero-parietal), -31 (midline central to right superior antero-parietal), -30 (midline central to right postero-parietal), and 27 (left mid-parietal to left superior antero-parietal). The ERC "noise" distribution had a mean of 0 and a standard deviation of 6.3. There were no significant ERCs for the Incipient-minus-Full-Fatigue subtraction.

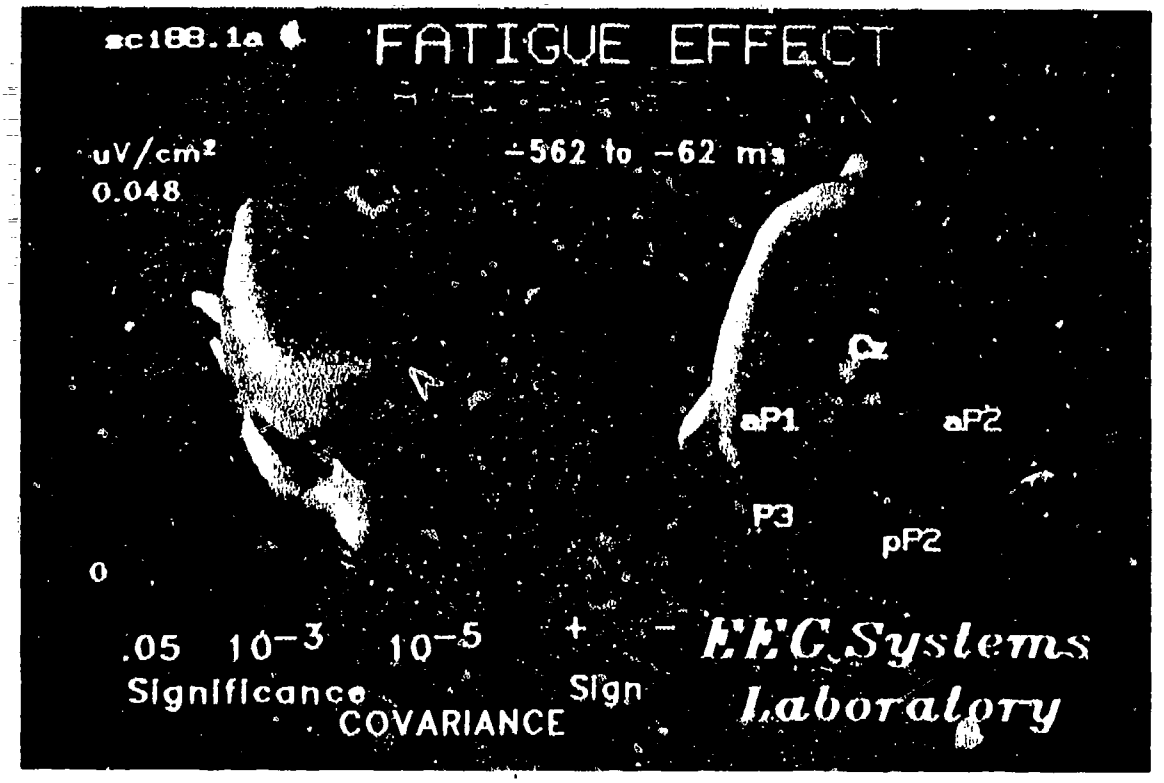

Figure 26B

Event-related covariance (ERC) patterns characterizing the prestimulus *difference* between Alert and Incipient Fatigue conditions from front (left) and top-of-head (right) perspectives. ERCs were computed from Alert-minus-Incipient-Fatigue LDs (Figure 26A; solid line) across the -562 to -62 msec prestimulus interval shown in Figure 26A. The width of a line shows the significance of the covariance between two electrodes. Violet lines represent positive covariances, while blue lines represent negative covariances. The midline central electrode, overlying the motor and premotor cortices, significantly covaries with left mid-parietal and right postero-parietal electrodes, and left and right superior antero-parietal, electrodes. This suggests that incipient fatigue selectively affected cortical areas responsible for preparing for a response, and maintaining the two visually presented numbers in working memory.

The N125 LD peak in the response trial set grand-average was highly localized to the midline parietal site due to the Laplacian transformation. Its amplitude declined slightly (3.1 to 2.9 $\mu V/ cm^2$) from the Alert to Incipient Fatigue conditions, and then increased slightly in the Full Fatigue condition (3.3 $\mu V/ cm^2$).

For the interval spanning the stimulus-locked N125 peak, none of the ERCs that were computed from the Alert-minus-Incipient-Fatigue subtraction LDs (Fig. 27A) were significant (Fig. 27B). For the Incipient-minus-Full-Fatigue subtraction, there was only one significant ERC, between the left and right postero-parietal sites (not shown). There were too few trials in the no-response trial set to see the N1 peak against the noise.

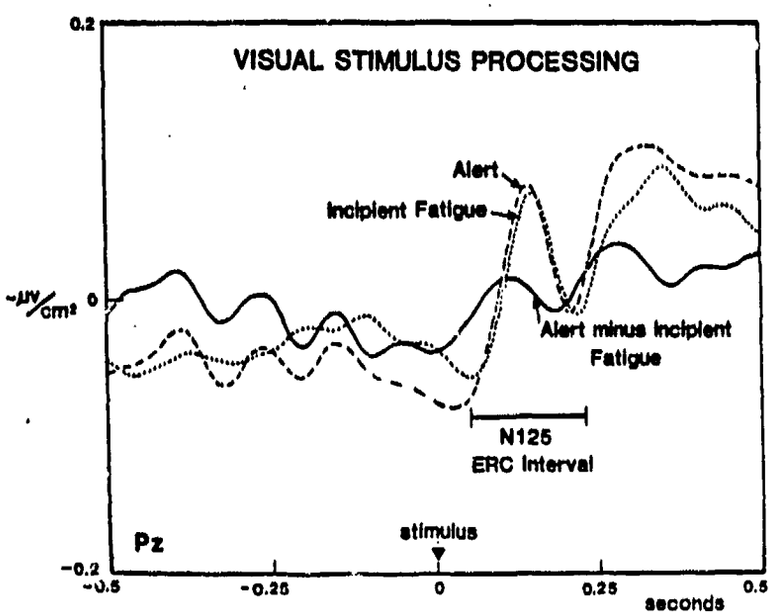

Figure 27A

Alert (562 trials) (dashed line), Incipient Fatigue (517 trials) (dotted line), and Alert-minus-Incipient-Fatigue grand-average LDs (solid line) of the midline mid-parietal (Pz) electrode, showing the N125 peak following presentation of the visual stimulus. The amplitude of the N125 did not differ between the Alert and Incipient Fatigue conditions.

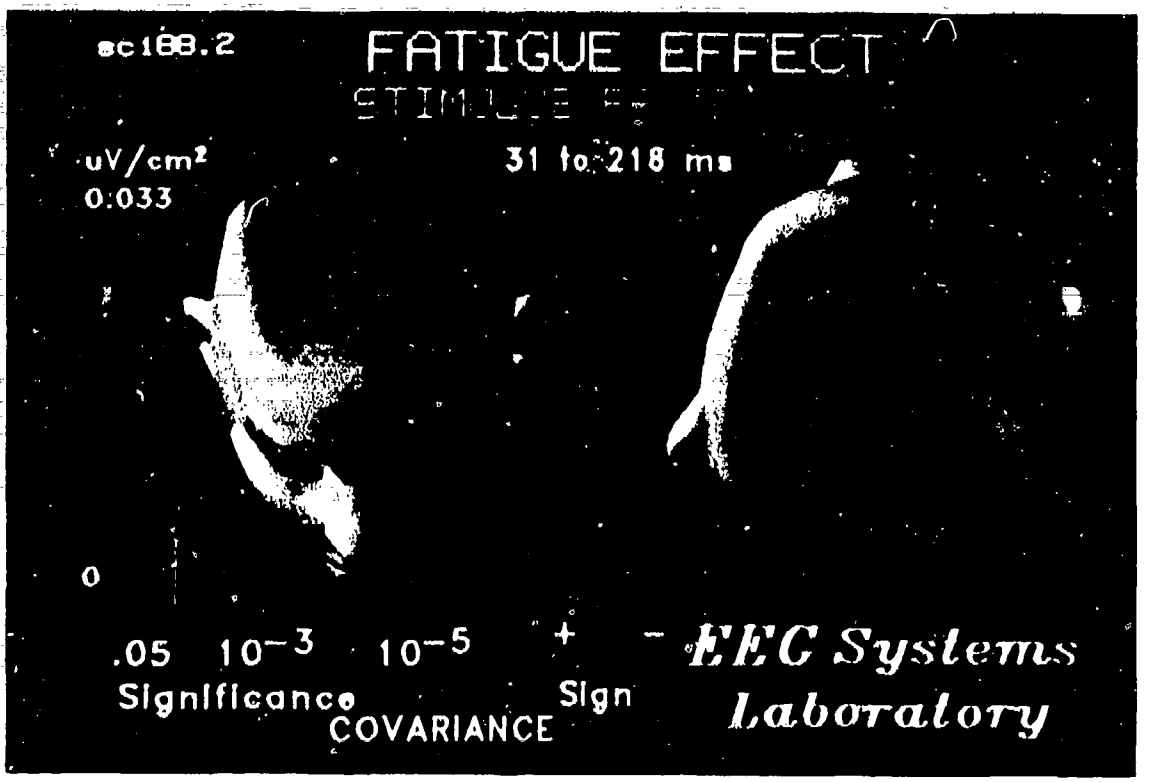

Figure 27B

There were no significant ERCs during the N125 interval. ERCs were computed from Alert-minus-Incipient-Fatigue LDs (Figure 27A; solid line) during the 31 to 218 msec post-stimulus interval spanning the N125 peak shown in Figure 27A. This suggests that visual stimulus processing was not affected during the early stage of fatigue.

The amplitude of the P380 in the no-response trial set significantly decreased across alertness conditions ($F=7.3$, $df=2,12$, $p<.01$). Scheffe post-hoc tests revealed that the amplitude of P380 was significantly smaller in the Full Fatigue average than in the Alert average ($F=7.3$, $df=2,12$, $p<.01$). The decrease in P380 amplitude from the Alert to the Incipient Fatigue condition did not reach statistical significance (Fig. 28A).

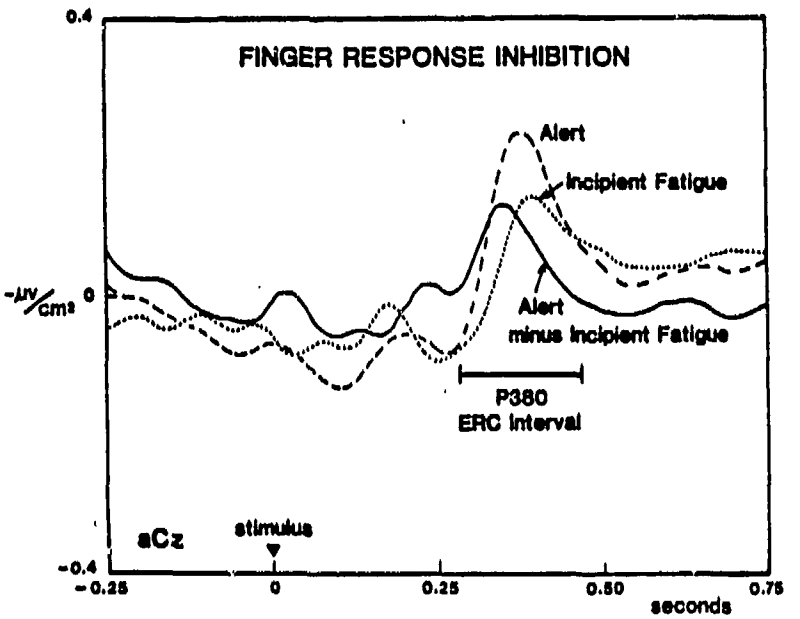

Figure 28A

Alert (243 trials) (dashed line), Incipient Fatigue (250 trials) (dotted line), and Alert-minus-Incipient-Fatigue grand-average LDs (solid line) of the midline antero-central (aCz) electrode for the response inhibition ("no-press") trials. The decrease in amplitude of the P380 peak from Alert to Incipient-Fatigue conditions was not significant.

Significant ERCs from the P380 Alert-minus-Incipient-Fatigue subtraction, in the no-response trial set, were observed between the midline antero-central, right antero-parietal and right postero-parietal sites (Fig. 28B). The values of the three significant ERCs were: -19 (midline antero-central to right inferior antero-parietal), 19 (midline antero-central to right postero-parietal), and -15 (right postero-parietal to right inferior antero-parietal). The mean and standard deviation of the ERC "noise" distribution were 0 and 2.8, respectively. No significant ERCs were found for the Incipient-minus-Full-Fatigue P380 LD.

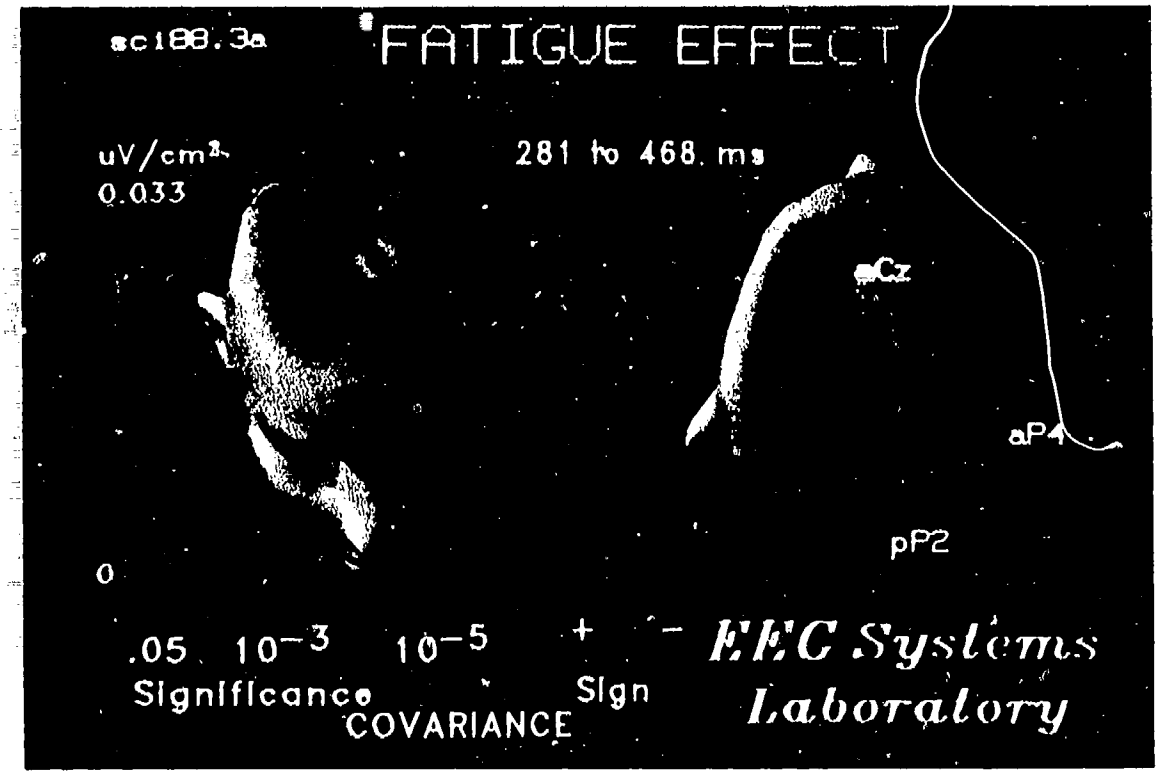

Figure 28B

"No-press" ERC patterns characterizing the *difference* between Alert and Incipient Fatigue from front (left) and top-of-head (right) perspectives. ERCs were computed from Alert-minus-Incipient-Fatigue LDs (Figure 29a, solid line) during the 281 to 468 msec post-stimulus interval. The triangle involving right inferior antero-parietal, right postero-parietal, and midline antero-central electrodes may reflect the effects of fatigue on cortical systems responsible for matching the current stimulus number with the one presented two trials back and then inhibiting the response.

Pattern classification procedures were used to measure the trial-by-trial discriminability of Alert from Incipient Fatigue prestimulus data, and to provide a summary index of differences between subjects. A two-layered adaptive "neural network" algorithm was used for the analysis. Single-trial ERCs, computed for channel pairs of the ERC patterns from both subtracted and unsubtracted grand-average ERPs, were considered as possible variables. The ratio of observations (trials) to variables exceeded 10:1 in each analysis. In each case, five analyses were performed, each using four-fifths of the data for training and the remaining fifth for testing significance of the average test set classification was assessed by reference to the bimanual distribution.

The average test-set discrimination of Incipient Fatigue from Alert trials was 58% ($p<0.001$), where five separate equations were formed on four-fifths of the trials and tested on the remaining fifth. Discrimination was above 57% for three subjects, but was 49% (chance) for the other two. In a second analysis using just the trials from the latter two subjects, average test-set discrimination was 61% ($p<0.001$), implying that ERC differences between Alert and Incipient Fatigue conditions were distributed differently from those of the first three subjects. A third analysis using just the trials from the first three subjects (representing 75% of the total trials), yielded an average test-set discrimination of 62% ($p<0.001$). Finally, a fourth analysis was made using only trials from the one subject with the best classification in the five-subject and three-subject analyses. The average test-set discrimination of Incipient Fatigue from Alert trials was 81% ($p<0.001$).

5. *Discussion*

We have reported preliminary results of a study that used state-of-the-art technology to document neurophysiological activity associated with different aspects of perceptuomotor and cognitive function in five U.S. Air Force test pilots during three stages of alertness: full alert, incipient fatigue and full fatigue. Over one billion bytes of data were collected. We have summarized the results from the high-load visuomotor memory task (VMMT) for the different alertness conditions, and have discussed the results of event-related covariance (ERC) analysis of LDs from event-related potentials obtained by subtracting the grand-average 5-subject LDs from the different alertness states for the stimulus-registered event. We will present the results of the prestimulus-, response- and feedback-registered events of the VMMT, Follow-Up Rested Session, and the Auditory Monitoring and Critical and Subcritical Tracking Tasks in separate reports.

These first results are quite exciting in suggesting how fatigue may selectively affect areas of the brain implicated in higher cognitive functions. The N125 LD peak and corresponding ERC pattern during the first 200 msec of the visual stimulus processing were relatively unaffected. By contrast, the later response-inhibition ERC patterns, from about 280 to 470 msec poststimulus (and to some extent the P380 peak amplitude), clearly showed neurophysiological changes consequent to incipient fatigue. Consistent with results of a previous study in our laboratory of visuomotor performance [39], the midline antero-central focus of the P380 no-response trial ERC patterns may reflect changes in neural systems responsible for motor inhibition. This electrode overlies supplementary motor and premotor cortices involved in the highest level of control of voluntary movements [50,64].

The highly specific temporal (LD peaks) and spatial (ERC patterns) changes associated with time-on-task suggest that the patterns are due to localized changes in areas of association cortex, and not to anatomically diffuse changes associated with decreased overall arousal.

We must also emphasize that while the ERC patterns reported here suggest fatigue-related degradation of functional coordination between immediately underlying cortical regions, the actual neural sources of the ERC patterns are, in fact, not yet known. Determining the distributed source network suggested by the scalp ERC patterns is the major focus of our current technical efforts.

The present results, analyses of the remaining data, and source localization studies will all elucidate the differential effects of incipient fatigue on areas of the brain implicated in higher cognitive functions. When these analyses are completed, it may be possible to specify studies leading to the design of on-line devices for predicting "transient cognitive lapses" and performance decrements resulting from operational fatigue. The same technology could be applied to predict acceleration-induced loss of consciousness episodes in high performance aircraft.

LITERATURE CITED

[1] Gevins, A.S., Zeitlin, G.M., Yingling, C., Doyle, J., Dedon, M., Henderson, J., Schaffer, R., Roumasset, J. & Yeager, C. (1979) EEG patterns during "cognitive" tasks. Part 1: Methodology and analysis of complex behaviors. *Electroencephalogr. clin. Neurophysiol., 47,* 693-703.

[2] Gevins, A.S., Zeitlin, G., Doyle, J., Schaffer, R. & Callaway, E. (1979) EEG patterns during "cognitive" tasks. Part 2: Analysis of controlled tasks. *Electroencephalogr. clin. Neurophysiol., 47,* 704-710.

[3] Gevins, A.S., Zeitlin, G.M., Doyle, J.C., Schaffer, R.E., Yingling, C.D., Yeager, C.L. & Callaway, E. (1979) EEG correlates of higher cortical functions. *Science, 203,* 665-668.

[4] Gevins, A.S., Doyle, J.C., Schaffer, R.E., Callaway, E. & Yeager, C. (1980) Lateralized cognitive processes and the electroencephalogram. *Science, 207,* 1005-1008.

[5] Gevins, A.S., Doyle, J., Cutillo, B.A., Schaffer, R., Tannehill, R., Ghannam, J., Gilcrease, V. & Yeager, C. (1981) Electrical potentials in human brain during cognition: New method reveals dynamic patterns of correlation of human brain electrical potentials during cognition. *Science, 213,* 918-922.

[6] Gevins, A.S., Schaffer, R.E., Doyle, J.C., Cutillo, B.A., Tannehill, R.S. & Bressler, S.L. (1983) Shadows of thought: Rapidly changing, asymmetric brain-potential patterns of a brief visuomotor task. *Science, 220,* 97-99.

[7] Gevins, A.S., Doyle, J.C., Cutillo, B.A., Schaffer, R.E., Tannehill, R.S., Bressler, S.L. & Zeitlin, G. (1985) Neurocognitive pattern analysis of a visuomotor task: Low-frequency evoked correlations. *Psychophysiology, 22,* 32-43.

[8] Gevins, A.S., Morgan, N.H., Bressler, S.L., Greer, D.S., Costales, B., Smith, K. & Faucette, R. (1987, In press) A fourth generation data collection and analysis system for brain research. *Proc. NATO Aerospace Medical Panel Symposium,* Trondheim, Norway.

[9] Gevins, A.S. (1987) Overview of computer analysis. In A. Gevins & A. Remond (Eds.), *Handbook of Electroencephalography and Clinical Neurophysiology: Methods of Analysis of Brain Electrical and Magnetic Signals (Vol. 1).* Amsterdam, Elsevier, pp. 31-83.

[10] Greer, D.S. & Gevins, A.S. (In preparation) Spatial deblurring of scalp recorded brain potentials using an optimal Laplacian operator.

[11] Gevins, A.S. & Morgan, N.H. (1986) Classifier-directed signal processing in brain research. *IEEE Trans. Biomed. Engr., BME-33* (12), pp. 1054-1068.

[12] Gevins, A.S. (1987) Obstacles to Progress. In A. Gevins & A. Remond (Eds.), *Handbook of Electroencephalography and Clinical Neurophysiology: Methods of Analysis of Brain Electrical and Magnetic Signals (Vol. 1).* Amsterdam, Elsevier, pp. 665-673.

[13] Gevins, A.S. (1986) Neurocognitive pattern analysis of auditory and visual information. *Interim Report, AFOSR Contract F49620-84-K-0008,* February.

[14] McGillem, C., Aunon, J. & Childers, D. (1981) Signal processing in evoked potential research: Applications of filtering and pattern recognition. *CRC Crit. Rev. Bioengr., 6* (3), 225-265.

[15] McGillem, C. & Aunon, J. (1987) Analysis of event-related potentials. In A. Gevins & A. Remond (Eds.), *Handbook of Electroencephalography and Clinical Neurophysiology: Methods of Analysis of Brain Electrical and Magnetic Signals (Vol. 1).* Amsterdam, Elsevier, pp. 131-169.

[16] De Weerd, J.P.C.M. (1981) *Estimation of evoked potentials: a study of a posteriori "Wiener" filtering and its time-varying generalization.* Doctoral dissertation, Katholieke Universiteit te Nijmegen, The Netherlands, Krips Repro Meppel.

[17] Gevins, A.S. (1984) Analysis of the electromagnetic signals of the human brain: milestones, obstacles and goals. *IEEE Trans. Biomed. Engr., BME-31* (12), 833-850.

[18] Gevins, A.S., Morgan, N.H., Bressler, S.L., Doyle, J.C., Cutillo, B.A. (1986) Improved ERP estimation via statistical pattern recognition. *Electroencephalogr. clin. Neurophysiol., 64,* 177-186.

[19] Morgan, N.H., & Gevins, A.S. (1986) Wigner distributions of human event-related brain signals. *IEEE Trans. Biomed. Engr., BME-33* (1), 66-70.

[20] Claasen, T.A.C.M. & Mecklenbrauker, W.F.G. (1980) The Wigner distribution — a tool for time-frequency signal analysis. *Phillips J. of Research, 35* (3), 217-250.

[21] Janse, C.P. & Kaiser, J.M. (1983) Time-frequency distributions of loudspeakers: the application of the wigner distribution. *J. Audio Engr. Soc., 31* (4), 198-223.

[22] Hjorth, B. (1975) An on-line transformation of EEG scalp potentials into orthogonal source derivations. *Electroencephalogr. clin. Neurophysiol., 39,* 526-530.

[23] Hjorth, B. (1980) Source derivation simplifies topographical EEG interpretation. *Am. J. EEG Technol., 20,* 121-132.

[24] Nunez, P.L. (1981) *Electric Fields in the Brain: The Neurophysics of EEG.* Oxford University Press, New York.

[25] Thickbroom, G.W., Mastaglia, F.L., Carroll, W.M. & Davies, H.D. (1984) Source derivation: application to topographic mapping of visual evoked potentials. *Electroencephalogr. clin. Neurophysiol., 59,* 279-285.

[26] Helmholtz, H. (1853) Ueber einige Gesetze der Vertheilung elektrischer Stroeme in korperlichen Leitern, mit Anwendung auf die thierischelek- trischen Versuche. *Ann. Phys. Chem., 29,* 211-233, 353-377.

[27] Freeman, W.J. (1980) Use of spatial deconvolution to compensate for distortion of EEG by volume conduction. *IEEE Trans. Biomed. Engr., BME-2* (8) 421-429.

[28] Nicholas, P. & Deloche, G. (1976) Convolution computer processing of the brain electrical image transmission. *Int. J. Bio-Med. Computing, 7,* 143-159.

[29] Hosek, R.S. (1970) *An experimental and theoretical analysis of effects of volume conduction in a nonhomogeneous medium on scalp and cortical potentials generated in the brain.* Unpublished Dissertation, Marquette University, Biomedical Engineering.

[30] Kavanagh, R.N., Darcey, T.M., Lehmann, D. & Fender, D.H. (1978) Evaluation of methods for three-dimensional localization of electrical sources in the human brain. *IEEE Trans. Biomed. Engr., BME-24* (5), 421-429.

[31] Fender, D.H. (1987) Source localization of brain electrical activity. In Gevins, A. & Remond, A. (Eds.), *Handbook of Electroencephalography and Clinical Neurophysiology, Vol. 1: Methods of Analysis of Brain Electrical and Magnetic Signals.* Elsevier, Amsterdam, pp. 355-403.

[32] Cooper, R., Osseltan, J.W. & Shaw, J.C. (1980) *EEG Technology.* (3rd Ed.). Butterworth, London.

[33] Curry, S., Moffitt, F.H., Symes, D. & Baumrind, S. (1982) Family of calibrated stereometric cameras for direct intra-oral use. *SPIE Proc., 361,* 7-14.

[34] Baumrind, S. & Curry, S. (1984) Merging of data from different records in craniofacial research and treatment. *Handbook of the 1984 Workshop on Non-topographic Photogrammetry.* American Society of Photogrammetry, July, 35-46.

[35] Geddes, L.A. & Baker, L.E. (1967) The specific resistance of biological material — A compendium of data for the biomedical engineer and physiologist. *Med. Biol. Engr., 5,* 271-293.

[36] Todd, T.W. (1924) Thickness of the male white cranium. *Anatom. Rec., 27,* 245-255.

[37] Todd, T.W. & Kuenzel, W. (1924) The thickness of the scalp. *J. Anat., 58,* 231-249.

[38] Gevins, A.S., Morgan, N.H., Bressler, S.L., Cutillo, B.A., White, R.M., Illes, J. Greer, D.S., Doyle, J.C. & Zeitlin, G.M. (1987) Human neuroelectric patterns predict performance accuracy. *Science, 235,* 580-585.

[39] Gevins, A.S., Bressler, S.L., Morgan, N.H., Cutillo, B.A., White, R.M., Greer, D. & Illes, J. (Submitted) Event-related covariances during a bimanual visuomotor task, Part I: Methods and analysis of stimulus- and response-locked data. *Electroencephalogr. clin. Neurophysiol.*

[40] Gevins, A.S., Cutillo, B.A., Bressler, S.L., Morgan, N.H., White, R.M., Illes, J. & Greer, D. (Submitted) Event related covariances during a bimanual visuomotor task, Part II: Preparation and feedback. *Electroencephalogr. clin. Neurophysiol.*

[41] Gevins, A.S. (1987) Correlation analysis. In A. Gevins & A. Remond (Eds.), *Handbook of Electroencephalography and Clinical Neurophysiology, Vol. 1: Computer Analysis of Brain Electrical and Magnetic Signals.* Amsterdam, Elsevier, pp. 171-193.

[42] Efron, B. (1970) *The Jacknife, the Bootstrap, and Other Resampling Plans.* SIAM: Philadelphia.

[43] Bressler, S.L. (1987) Relation of olfactory bulb and cortex. I. Spatial variation of bulbo-cortical interdependence, *Brain Res., 409,* 285-293.

[44] Bressler, S.L. (1987) Relation of olfactory bulb and cortex. II. Model for driving of cortex by bulb, *Brain Res., 409,* 294-301.

[45] Freeman, W.J. (1975) *Mass Action in the Nervous System.* New York, Academic Press.

[46] Walter, W.G. (1967) Slow potential changes in the human brain associated with expectancy, decision and intention. *Electroencephalogr. clin. Neurophysiol., 26,* 123-130.

[47] Rohrbaugh, J.W., Syndulko, K., Sanquist, T.F. & Lindsley, D.S. (1980) Synthesis of the contingent negative variation brain potential from arm contingent stimulus and motor elements. *Science, 208,* 1165-1168.

[48] Macar, F. & Besson, M. (1985) Contingent negative variation in processes of expectancy, motor preparation and time estimation. *Biol. Psychol., 21,* 293-308.

[49] Stuss, D.T & Benson, D.F. (1986) *The Frontal Lobes.* Raven Press, New York.

[50] Roland, P.E., Meyer, E., Shibasaki, T., Yamamoto, Y.L. & Thompson, C.J. (1982) Regional cerebral blood flow changes in cortex and basal ganglia during voluntary movements in normal human volunteers. *J. Neurophysiol., 48,* 467-480.

[51] Goldberg, G. (1985) Supplementary motor area structure and function: Review and hypotheses. *Behav. Brain Sci., 8,* 567-616.

[52] Evarts, E., Shinoda, Y. & Wise, S. (1984) *Neurophysiological Approaches to Higher Brain Functions.* New York, Wiley.

[53] Johnson, R., Jr. (1980) Event-related potentials accompanying voluntary movement in the rhesus monkey. In: H.H. Kornhuber and L. Deecke (Eds.), *Motivation, Motor and Sensory Processing of the Brain, Prog. Brain Res., 54,* 70-76.

[54] Mesulam, M.M. (1981) A cortical network for directed attention and unilateral neglect. *Ann. Neurol., 10,* 309-325.

[55] Johnson, R., Jr. & Donchin, E. (1985) Multiple P300s: Multiple P300s elicited by a single stimulus. *Psychophysiol., 22,* 182-194.

[56] Ruchkin, D.S. & Sutton, S. (1983) Positive slow wave and P300: Association and disassociation. In: A. Gaillard and W. Ritter (Eds.), *Tutorials in ERP Research: Endogenous Components.* Amsterdam, North-Holland, 233-250.

[57] Gevins, A.S. & Cutillo, B.A. (1986) Signals of Cognition. In: F. Lopes da Silva, W. Storm van Leeuwen & A. Remond (Eds.), *Application of Computer Analysis to EEG. Handbook of Electroencephalography and Clinical Neurophysiology (Vol. 2).* Amsterdam, Elsevier, 335-381.

[58] Gevins, A.S. (1983) BEP evidence for lateralization of higher cognitive functions. In: J.B. Hellige (Ed.), *Cerebral Hemisphere Asymmetry: Method, Theory and Application.* New York, Praeger Press, 335-382.

[59] Jex, H.R. (1978) Defining and measuring perceptual-motor workload in manual control tasks. *Tech. Report 1104-1,* Systems Technology Inc.

[60] Allen, R.W. & Jex, H.R. (1971) Visual-motor response of crewmen during a simulated 90-day space mission as measured by the critical task battery. *Paper No. 100a,* Systems Technology Inc., May.

[61] Sternberg, S., Monsell, S., Knoll, R. & Wright, C. (1978) The timing of rapid movement sequences. In: G. Stelmach (Ed.), *Information Processing in Motor Control and Learning.* New York, Academic Press, 117-152.

[62] Gevins A.S. (In Press) Recent advances in neurocognitive pattern analysis. In: E. Basar (Ed.), *Dynamics of Sensory and Cognitive Processing in the Brain.* New York, Springer-Verlag.

[63] Gevins, A.S. Bressler, S.L., Morgan, N.H., White, R.M., Greer, D.S. & Illes, J. (1987, In Press) Neurophysiological precursors of accurate visuomotor performance. *Proc. NATO Aerospace Medical Panel Symposium.* Trondheim, Norway.

[64] Foit, A., Larsen, B., Hattori, S., Skinhoj, E. & Lassen, N.A. (1980) Cortical activation during somatosensory stimulation and voluntary movement in man: A regional blood flow study. *Electroencephalogr. clin. Neurophysiol., 50,* 426-436.

CERTIFICATION OF TECHNICAL DATA CONFORMITY

The Contractor, EEG SYSTEMS LABORATORY, hereby certifies that, to the best of its knowledge and belief, the technical data delivered herewith under Contract No. F49620-84-K-0008 is complete, accurate, and complies with all requirements of the contract.

Date: 23AUG87

Alan S. Gevins, Director